Molecular Dynamics of C99-Bound γ-Secretase Reveal Two Binding Modes with Distinct Compactness, Stability, and Active-Site Retention: Implications for Aβ Production

Dehury, Budheswar; Tang, Ning; Kepp, Kasper Planeta

Published in:
Biochemical Journal

Link to article, DOI:
10.1042/BCJ20190023

Publication date:
2019

Document Version
Peer reviewed version

Molecular Dynamics of C99-Bound γ-Secretase Reveal Two Binding Modes with Distinct Compactness, Stability, and Active-Site Retention: Implications for Aβ Production

Budheswar Dehury, Ning Tang, and Kasper P. Kepp*

Department of Chemistry, Technical University of Denmark, DK-2800 Kongens Lyngby, Denmark

*Corresponding author: Kasper P. Kepp. E-mail: kpj@kemi.dtu.dk. Phone: +045 45252409

Abstract

The membrane protease γ-secretase cleaves the C99 fragment of the amyloid precursor protein (APP) thus producing the Aβ peptides central to Alzheimer's disease. Cryo-electron microscopy has provided the topology but misses the membrane and loop parts that contribute to substrate binding. We report here an essentially complete atomic model of C99 within wild-type γ-secretase that respects all the experimental constraints and additionally describes loop, helix, and C99 substrate dynamics in a realistic all-atom membrane. Our model represents the matured auto-cleaved state required for catalysis. From two independent 500-ns molecular dynamics simulations, we identify two conformation states of C99 in equilibrium, a compact and a loose state. Our simulations provide a basis for C99 processing and Aβ formation and explain production of longer and shorter Aβ, as the compact state retains C99 for longer and thus probably trims to shorter Aβ peptides. We expect pathogenic presenilin mutations to stabilize the loose over the compact state. The simulations detail the role of the Lys53-Lys54-Lys55 anchor for C99 binding, a loss of helicity of bound C99, and positioning of Thr48 and Leu49 leading to alternative trimming pathways on opposite sides of the C99 helix in three-amino acid steps. The C99-binding topology resembles that of C83-bound γ-secretase without membrane but lacks a PS1-C99 β-sheet, which could be induced by C83's stronger binding. The loose state should be selectively disfavored by γ-secretase modulators to increase C99 trimming and reduce formation of longer Aβ, a strategy that is currently much-explored but has lacked a structural basis.

Keywords: γ-secretase; Aβ; Alzheimer's disease; C99; molecular dynamics; protein complex

Introduction

The 99-residue C-terminal fragment (C99) of the amyloid precursor protein (APP) is produced upon cleavage by β-secretase; C99 is subsequently cleaved by the enzyme complex γ-secretase, releasing the infamous amyloid-β peptides (Aβ) central to Alzheimer's Disease (AD)[1,2]. Aβ isoforms of different lengths are produced during the slow[3] consecutive trimming of C99 within γ-secretase[4–6]. The longer isoforms, notably $A\beta_{42}$, are particularly toxic and aggregation-prone and are enriched in the plaques of AD brains and thus considered central to the development of AD[7–9]. Understanding how Aβ isoforms of variable length are formed within the molecular architecture of the large γ-secretase complex is an outstanding challenge that will be central to efforts to modulate C99 processing and the associated Aβ profile by specific medicine, e.g. γ-secretase modulators[10,11].

During the last decade, various computational and experimental studies have explored the transmembrane domain (C99-TMD) structure and dynamics of C99[12–15]. Some studies have identified specific residues of the extra-membrane segment of C99 that may affect Aβ production, and some of these may change upon mutations leading to AD[16–18]. Because of the complications of studying disordered proteins in membranes, a structure of full-length membrane-bound C99 is unavailable, and just recently was a structure published of the shorter C83 analog bound to γ-secretase[19]. NMR-derived structures of the transmembrane domain of C99 (PDB ID: 2LP1) have been reported[15], but the full structure of C99 beyond the transmembrane (TM) region is yet to be unveiled.

γ-secretase, a membrane-embedded aspartate protease, is comprised of four subunits: nicastrin (NCT), the catalytic presenilin 1 (PS1) or its isoform presenilin 2 (PS2), anterior pharynx defective-1 (APH1), and presenilin enchancer-2 (PEN2)[20]. Presenilin is comprised of nine TM helices (TM1-9) and contains the two catalytic aspartate residues in TM6 (Asp-257) and TM7 (Asp-385) that are instrumental to substrate peptide bond hydrolysis of a large variety of type I

integral membrane proteins including APP and Notch[21]. γ-secretase is catalytically matured by auto-cleavage of PS1 to form the N-terminal fragment (NTF, TM1-6) and C-terminal fragment (CTF, TM7-9)[22]. PEN2 and APH1 interact with PS1 and have significant roles in the maturation and assembly of the γ-secretase complex[23]. Furthermore, NCT is comprised of a single TM in its C-terminal region and a large N-terminal extracellular domain (ECD), which can discriminate access of substrates to the active site by size-selective control[24].

Over the last four years, cryo-electron microscopic (cryo-EM) structures have described apo-γ-secretase at increasing resolution (PDB ID: 4UI2, 5A63, 5FN2, 5FN3, 5FN4 and 5FN5)[25–28]. New structures of Notch-100[29] and C83[19], bound to γ-secretase were published recently. The protein changes TM2 and TM6 conformation during substrate binding as expected from their special flexibility defining the open and closed states of the protein[30]; as new feature of the recent cryo-EM structure is that substrate binding induces a small strand segment in C83 and PS1 and extends the C83 trans-membrane helix[19]. Although foundational, the specific atomic motions underlying the density maps, the functionally important loops, the membrane's role in the conformational packing, and the effects of ambient temperature are not captured by the new structure, and it is also of interest to understand whether the natural, more weakly binding substrate C99 differs in its conformation from that of C83.

The mechanism of C99 cleavage depends on an intriguing interplay between loop and helix dynamics, with only the later clearly visible in the cryo-EM data[31,32]. Molecular dynamics (MD) simulations efficiently equilibrate all modes with fast time scales (such as water-protein interactions, water dynamics, and side chain rotamer states[33]), and provides qualitatively correct dynamics at high resolution for the important loop and helix motions, including the hinge bending critical to this protein complex[30], if their characteristic timescale of typically ~10-100 ns is covered[34,35]. Accuracy is limited by the realism of the chemical model, the sampling efficiency, and the physical force field. However, the first restriction applies also to the context-

and protocol-dependent experimental structures, and for the helix movements, the force field and sampling problem is small compared to e.g. protein folding[36–38]. More importantly, atomic-resolution dynamics are not achievable in any other way than from MD and thus MD has been instrumental in understanding proteins within realistic membrane environments[13,14,39,40].

As an example of the importance of accurate chemical models, maturation cleavage of the large loop between TM2 and TM6 is crucial for activity, but elusive in any cryo-EM studies since the loops are too disordered[4,41]. The direct role of loop maturation is well-understood from MD simulations showing that maturation leads to the two new dynamic fragments that enable access to the catalytic site and modulate the TM2-TM6 gate doors controlling C99 packing[30,42]. The Fit-Stay-Trim (FIST) mechanism[30,43] implies that a closer fit of C99 increases residence time and extends trimming, leading to shorter Aβ; this state is hypothesized to be disfavored relative to an open state by many PS1 mutations leading to increased $A\beta_{42}/A\beta_{40}$ ratios which directly correlate with clinical severity of disease[44].

We report here the first study of a complete molecular model of C99 within the essentially complete (except the experimentally elusive N-terminal loop of PS1) all-atom structure of γ-secretase. Our model respects all the available structural coordinates of γ-secretase and the major dynamics known, as validated below. We employed MD simulations of both the C99-γ-secretase complex and the apo-form of γ-secretase in a realistic membrane environment. We specifically accounted for the maturation cleavage of γ-secretase[45,46] which substantially affects the conformational flexibility of the protein complex and is required for activity[42]. We also analyzed the binding free energy of C99 to directly probe the stability of the different conformational states. We identify two major conformation states of C99, a loose and a compact state, which largely confirm the hypothesis of the FIST mechanism and rationalize the observation of long and short Aβ peptides that are centrally important to AD.

Computational methods

Model of C99 bound to γ-Secretase

The initial full-length C99 structure was obtained from a recent study[14]. The structure of C99 is sensitive to membrane lipid composition, and thus we used the structure of fragment 23−55 sampled by Dominguez et al. (2016)[40], which is in agreement with the experimental data. The N-terminal 1–22 and the N-terminal 56–99 residues were built using dihedral angles predicted via TALOS+[47], using the Cα, Cβ, C, N, and H chemical shifts reported for C99 in LMPG micelles[48]. The protonation state of each residue of the C99 model was defined using UCSF Chimera[49] and the model was optimized by modeling the missing side chains using WHAT-IF[50]. The complete C99 model was then docked with our previous established semi-open state of γ-secretase[30] to obtain the C99-γ-secretase complex, using the ClusPro server[51] with the two catalytic aspartate residues as restraints. This structure is complete except for the experimentally elusive and functionally unimportant N-terminal of PS1, which has no experimental template and thus cannot be modeled at acceptable accuracy. The obtained cluster with the maximum number of structures having low energy (**Supporting Information, Table S1**) was chosen for optimization in the pure lipid bilayer system.

MD simulation of γ-secretase and C99-γ-secretase in a lipid bilayer system

To construct the complete membrane model of the C99-bound γ-secretase, the initial coordinates of the membrane were obtained using the Position Protein in Membrane (PPM) server[52]. Then, the membrane-aligned structures were embedded into a membrane−solvent bilayer system using the CHARMM-GUI web server[53]. A homogeneous POPC lipid bilayer was generated around the protein by maintaining a water thickness of 20 Å using Monte Carlo randomization, and the system was neutralized by addition of Na^+ and Cl^- ions to a total concentration of 0.15 M NaCl.

The resulting protein-membrane structural model was subject to extensive quality control vs. experimental facts as detailed in the results and discussion below.

MD production simulations

All-atom MD simulations were performed with the TIP3P explicit water model[54] and the structure-balanced CHARMM36m force field[55] in the graphical processing unit version of GROMACS (2018.2)[56]. Non-bonded interactions were evaluated using a Verlet cut-off scheme, with both Coulomb and Lennard-Jones interactions having a cut-off of 12 Å. Particle Mesh Ewald summation was used for long-range electrostatic interactions, and hydrogen bond lengths were constrained using Linear Constraint Solver (LINCS) algorithm[57]. The complete protein−lipid−solvent system was minimized by steepest decent optimization, followed by six-step position-restrained equilibration for 500 picoseconds. During the first two steps, the system was equilibrated in a canonical (NVT) ensemble using Berendsen temperature coupling, and in the next four steps, equilibration was achieved within the isothermal−isobaric (NPT) ensemble.

After equilibration, 500 ns production simulations were carried out with a 2-femtosecond time step in an NPT ensemble using the Nose−Hoover thermostat and the Parrinello−Rahman barostat at 303.15 K and 1 atm, respectively. We have previously found[30] that it takes 200 ns to reach stable trajectories as estimated from the horizontal RMSD graphs vs. initial structures. In addition, the functionally important helix motions of PS1 are, as expected[33,35], well-sampled on a time scale of 100 ns after the first 200 ns required for equilibration, and a 500-ns simulation of the full system thus samples the central dynamics qualitatively well. In order to ensure this, we performed two complete 500-ns simulations using distinct initial random velocity seeds. As seen from the analysis below, these simulations are in essential agreement and serve as mutual confirmation. Both simulations were performed during 2018 using the graphical processing units of the high-performance-computing facility at the Technical University of Denmark.

Trajectory analysis

The obtained trajectories were analyzed using the built-in analysis tools of GROMACS version 2018.2[56]. The deuterium order parameters of the acyl chains, density of the membrane environment, area per lipid head group, and bilayer thickness were analyzed using GROMACS utility tools and FATSLiM[58] to ensure optimal quality control of the protein-membrane system. The backbone root-mean-square deviation (RMSD), Cα root-mean-square fluctuation (RMSF), and solvent-accessible surface area (SASA) were analyzed. All analysis presented in this work reflects the last, stable 300 ns of the simulations, since, as explained above, the first 200 ns are required to reach an equilibrated stable state. Ensemble-average clustering was performed using the clustering algorithm of Daura et al.[59] implemented in the *gmx cluster* tool of GROMACS with a cut-off 0.2 nm, applied to the last 300 ns of each simulation. Principal component analysis (PCA) and the corresponding collective motions were analyzed using the last 300 ns information of each simulation. Visual Molecular Dynamics v.1.9.3 (VMD)[60] was used for visualization of MD trajectories, and PyMOL version 2.0 was used for rendering of figures.

Estimation of Binding Free Energy of C99 to γ-secretase

The free energy of binding C99 to γ-secretase was determined using the *g_mmpbsa* tool[61], which employs molecular-mechanics based Poisson–Boltzmann Surface Area (MM/PBSA) calculations[62]. These energies were calculated for each of 100 frames extracted equidistantly from the last 300 ns of each MD trajectory. The total binding energy (ΔG_{bind}) is the average (with reported standard deviations from this average) of all 100 calculations. We used solute and solvent dielectric constants of 2 and 80, respectively. Energy decomposition was carried out to understand the contribution of individual amino acids to the total obtained binding energy.

Results and discussion

Structure and dynamics of C99-γ-secretase within a membrane

Despite significant advancements in the general structure of γ-secretase, many features of the C99 binding remains unknown[25,27,28,32]. A very recent cryo-EM structure of C83-bound γ-secretase in ice[19] published after we submitted our paper reveals important changes during substrate binding. Our MD simulations supplement with the underlying atomic dynamics causing these changes for the full C99 substrate in a relevant membrane environment at ambient temperature. The membrane cleavage of C99 leads to formation of Aβ and is therefore a cornerstone of structure-based attempts to understand AD and to develop causative medicine against the disease.

Based on the initial docked conformations of C99 obtained from ClusPro, PS1 and NCT consistently interacted strongly with the substrate (**Figure S1** and **Table S2**). After MD simulation, the C99 binding pocket was comprised of TM2 (Gln127-Tyr156), TM3 (Val161-Tyr189) and TM5 (Leu219-Tyr240), where TM2, TM6 (Glu243-Val261), TM9 (Ala434-His463) and the PAL motif (Pro433-Ala434-Leu435) interact closely with the substrate. The positioning of the C99-TMD (Gly29–Leu52) within the membrane is of particular interest and is analyzed further in the next sections. The TMD is strongly fixated by the positively charged lysines Lys53-Lys54-Lys55 of C99. Cleavage assays in cells and alanine-scanning mutagenesis suggest a central role of this motif in controlling substrate cleavage[63,64]. Other non-bonded contacts with C99-TMD are shown in **Table S2**. The details of each subunit interaction with C99 resulting from full MD equilibration is discussed further in the next section.

One of the novelties of our work is to provide the membrane context of the substrate-binding. To test the quality and realism of our protein-membrane model, we evaluated the membrane order parameters (S_{Cd}) of the head groups and acyl chains of the lipid tails, the density of membrane, and properties of the POPC bilayer. The membrane order parameters (**Figure S2**)

estimate the configurational flexibility of the lipids as a function of position within the lipid chain. The order parameters of the lipid head groups in **Figure S2** as well as the calculated membrane area per lipid molecule and membrane thickness (**Figure S3**) show excellent agreement with the typical experimental values of these properties and also agree well with previous MD studies[65,66]. Most importantly, they provide quality control that the membrane system retains its conformational integrity during the simulations.

The equilibrated membrane-structure can be compared with experimental structures without the membrane. The RMSD for the PS1 Cα atoms between the most representative computed structure from cluster analysis and the experimental apo-structure 5FN2[27] is 1.55 and 1.49 Å for simulation 1 and simulation 2 (**Figure S4**). The corresponding simulated apo-structures displayed RMSDs of 1.30 and 1.57 Å, respectively. Compared to the new cryo-EM structure of C83-γ-secretase (PDB ID 6IYC) [19], with the RMSD for Cα atoms of PS1 is 1.81 Å and 1.88 Å, respectively, for simulation 1 and 2. The MD-equilibrated membrane-bound topology is thus in very good agreement with the topology of the cryo-EM structure for the parts that are not missing in the experimental structure, but also differs in some parts close to the membrane and C99, as discussed below.

Our complete structural model is shown in **Figure 1A**, with Na^+ and Cl^- ions shown but water molecules removed for clarity. **Figure 1B** shows the RMSD from the start structure at 200-500 ns during the two independent 500-ns simulations of this system. The full complex displays stable states after 200 ns, implying that we can collect statistics from the last 300 ns, as done below. The simulations reveal important dynamics of the individual subunits and C99 discussed in further detail below. The most important of these is arguably the distance between the two catalytic aspartate residues (measured as the Cα-Cα distance) which displays considerable dynamic variation during the simulations in both cases (**Figure 1C**). This and other dynamic variations are relevant to the C99 binding and processing and are analyzed further below.

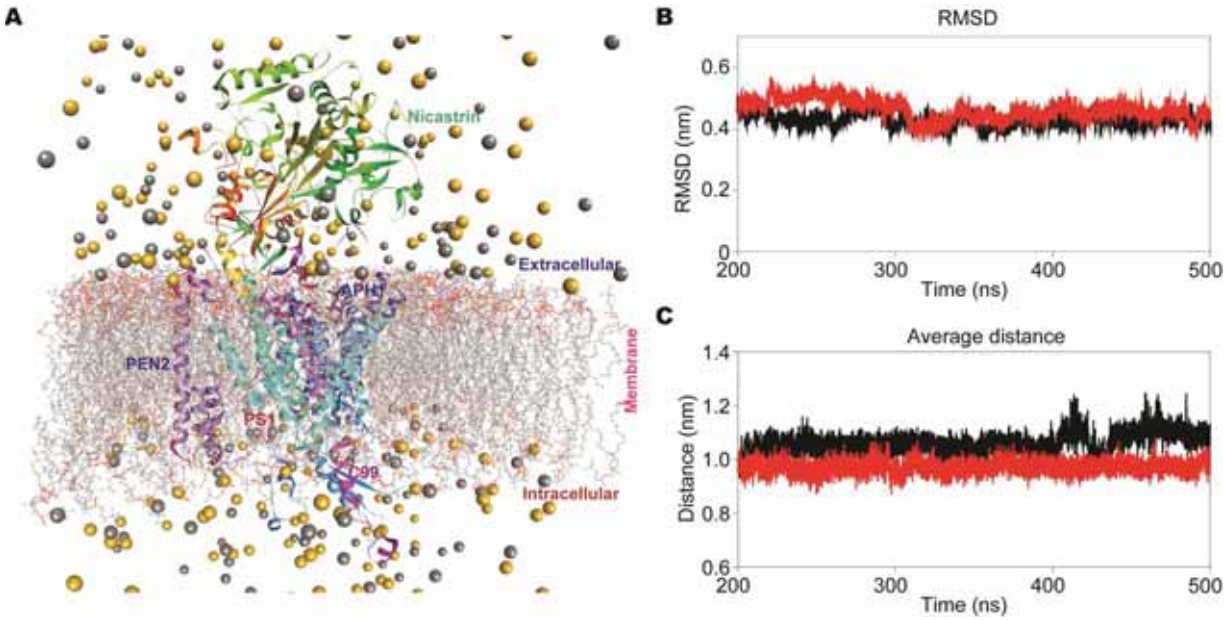

Figure 1. (A) Complete structural model of membrane-bound γ-secretase with the C99 fragment bound. **(B)** Stability of trajectories based on the root-mean squared deviation (RMSD) of the backbone atoms. **(C)** Average distance between the catalytic Asp-257 and Asp-385 Cα atoms of C99-γ-secretase during the last 300 ns of all-atoms MD simulation.

Individual subunit contributions to C99-γ-secretase dynamics

To understand the underlying dynamics of system in more detail, we analyzed the structural changes (as measured by coordinate RMSD plots) and fluctuations in atomic positions of all four subunits and C99 separately with respect to the initial pre-equilibrated structure. **Figure 2A-2E** shows the structural variation for NCT, PS1, APH1, PEN2, and C99 along the equilibrated part of the simulation trajectories for simulation 1 (black curves) and 2 (red curves). Both systems reach dynamically stable states as seen from the predominant horizontal plots. However, the RMSD plot of PS1 (**Figure 2B**) indicates two distinct conformations in the two simulations, despite minor differences in the other subunits (**Figure 2A**, **2C**, **2D**). Finally, C99 displays structural variation within the overall enzyme complex, indicating that C99 is flexible at the

membrane interface when bound (and probably more flexible than C83, see below), which may be important to the generation of different types of Aβ peptides, as explored in more detail below.

Figure 2F-2J shows the corresponding thermal fluctuations averaged over the last 300 ns, divided into residue. We identify high mobility of the NCT extracellular loop region and C-terminal and some, but comparatively little mobility of TMs (**Figure 2F**). The high thermal fluctuation of the C-terminal is a common feature also seen in APH1 (**Figure 2H**) and PEN2 (**Figure 2J**). TM5-7 of APH1 and some parts of PEN2 exhibit fluctuations due to their exposure to the membrane lipids and fewer protein–protein contacts, and display very similar dynamic behavior in both simulations. The dynamics of PEN2 and APH1 compared to the dynamics of the other two subunits is intriguing: PS1 (**Figure 2G**) shows major fluctuations across its sequence, especially of TM2, TM9, the hydrophilic loop 1 (HL1), and the large maturation-cleaved cytosolic loop between TM6 and TM7 (HL2). The maturation is instrumental in producing the distinct conformational variability of PS1, as evident also from comparative PS1-alone simulations with and without maturation cleavage[42]. The TMs of PS1 that are close to PEN2 and APH1 γ–secretase display less mobility. Previous studies suggest that PEN2 and APH1 stabilize the catalytic site[67], and the compact dynamic states of these subunits (**Figure 2H, 2I**) probably cause this tendency. Specifically, we find that the major helix of NCT forms important contacts with TM3–TM4 (Tyr195-His214) of PS1, and the N-terminal region of PEN2 interacts with the PS1 near the catalytic site (**Supporting Information, Figure S5**). HL1 interacted with the TM of C99 and displayed high flexibility during the MD simulations indicating a role in substrate recognition. This corroborates earlier studies by Tomita et al.[68] and is also partly evident from the cryo-EM structure of PS1-γ-secretase with C83[19], although the thermal motions are expected top be much smaller at cryo temperature and thus possibly lead to only one bound conformation state.

The higher RMSF of TM2 and TM6 suggests that collective motions modulate the relative orientation of these helices within the membrane when C99 is bound. Tominaga et al.[69] found that changes in the distance between TM6 and TM7 (Val379-Thr399) relate to $A\beta_{42}$ production, signifying the critical role of TM6 conformation in C99 processing. We have previously shown[30] that TM2 and TM6 form gate doors to the active site, controlled by the mature HL2 acting as a plug preventing access to this gate; however these and all other structural findings reflect γ-secretase without C99, and thus our new results suggest that the most important TM motions are present both with and without substrate bound, although their magnitude changes. Cryo-EM structures also indicate substantial motion of these helices[27], and at ambient temperature these tilt changes are major, as seen from the RMSF data in **Figure 2G**.

C99 within γ-secretase has a compact TM region but flexible membrane association

Our simulations also provide the first full-atom structural dynamics of C99 bound to γ-secretase in the membrane, as summarized by the RMSD and RMSF plots in **Figure 2E** and **2J**, respectively. The two statistically independent simulations qualitatively display similar thermal fluctuations. The disordered N-terminal residues (1-14) of C99 display some flexibility, but these motions monotonically decrease along the sequence of C99 as the membrane dampens C99 motions. We find that the C99-TMD, specifically residues 29–52, is completely dampened, such that dynamic control is exerted by the PS1 states.

The hinge G37-G38 region of the C99-TMD, speculated to be vital for processing by γ-secretase[12] displayed small variations, slightly larger than the neighboring, very fixed membrane residues. Previous MD simulation studies have shown that the GG hinge defines a dimerization motif and is thus conformation-wise important[13,40,70]. Both NMR and MD simulations studies imply that G37-G38 of C99 can act as dynamic hinges[13,15,71], where the "hinge-bending" presumably assists substrate binding within the γ-secretase active site[72]. The

C-terminal part of C99 outside the membrane was very flexible in both simulations but with larger thermal fluctuation in simulation 1 (black, **Figure 2J**). Circular dichroism (CD) spectroscopy and amide exchange experiments have shown that mutation of Thr43 and Thr48 to hydrophobic valines modulates the extent and direction of helix bending without altering the local flexibility at the ε-sites[73], but affecting the generation of $A\beta_{42}$ and $A\beta_{40}$[74]. Our results provide a plausible explanation of the altered cleavage as due to the large bending flexibility of the C99-TMD[75]. The bend motion profoundly affects the exact Asp-Asp distance dynamics within the catalytic site and thus probably the pattern of proteolytic processing. We conclude that there are minor fluctuations in C99-TMD once fit within the catalytic site, but major dynamics at the interface of the membrane interacting with the disordered N- and C-terminal parts of C99; the N-terminal part is not present in the new experimental cryo-EM structure of C83[19]. We show below that these membrane-protein dynamics give rise to two conformational states of bound C99 with distinct catalytic Asp-Asp distances, which can explain the two C99 cleavage pathways leading to Aβ and the production of shorter and longer peptides, which is elusive in the one-state C83 cryo-EM structure.

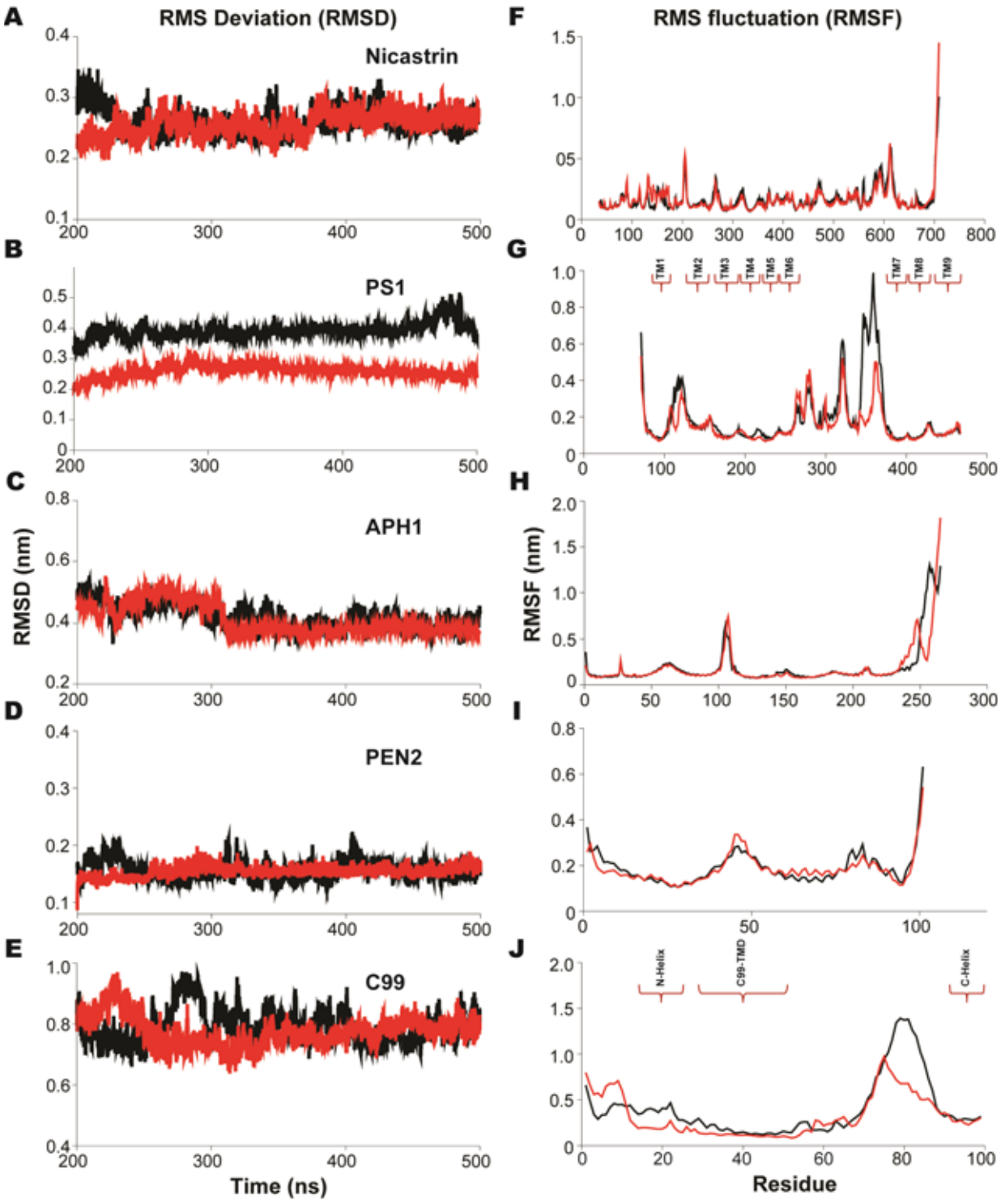

Figure 2. The root-mean-squared deviation relative to the initial prepared model (RMSD) and averaged root-mean-squared fluctuations (RMSF) of individual residue Cα atoms in C99-γ-secretase. **(A)** NCT RMSD; **(B)** PS1 RMSD; **(C)** APH1 RMSD; **(D)** PEN2 RMSD; **(E)** C99 RMSD; **(F)** NCT RMSF; **(G)** PS1 RMSF; **(H)** APH1 RMSF; **(I)** PEN2 RMSF; **(J)** C99 RMSF. Black and red colors represent simulation 1 and simulation 2, respectively.

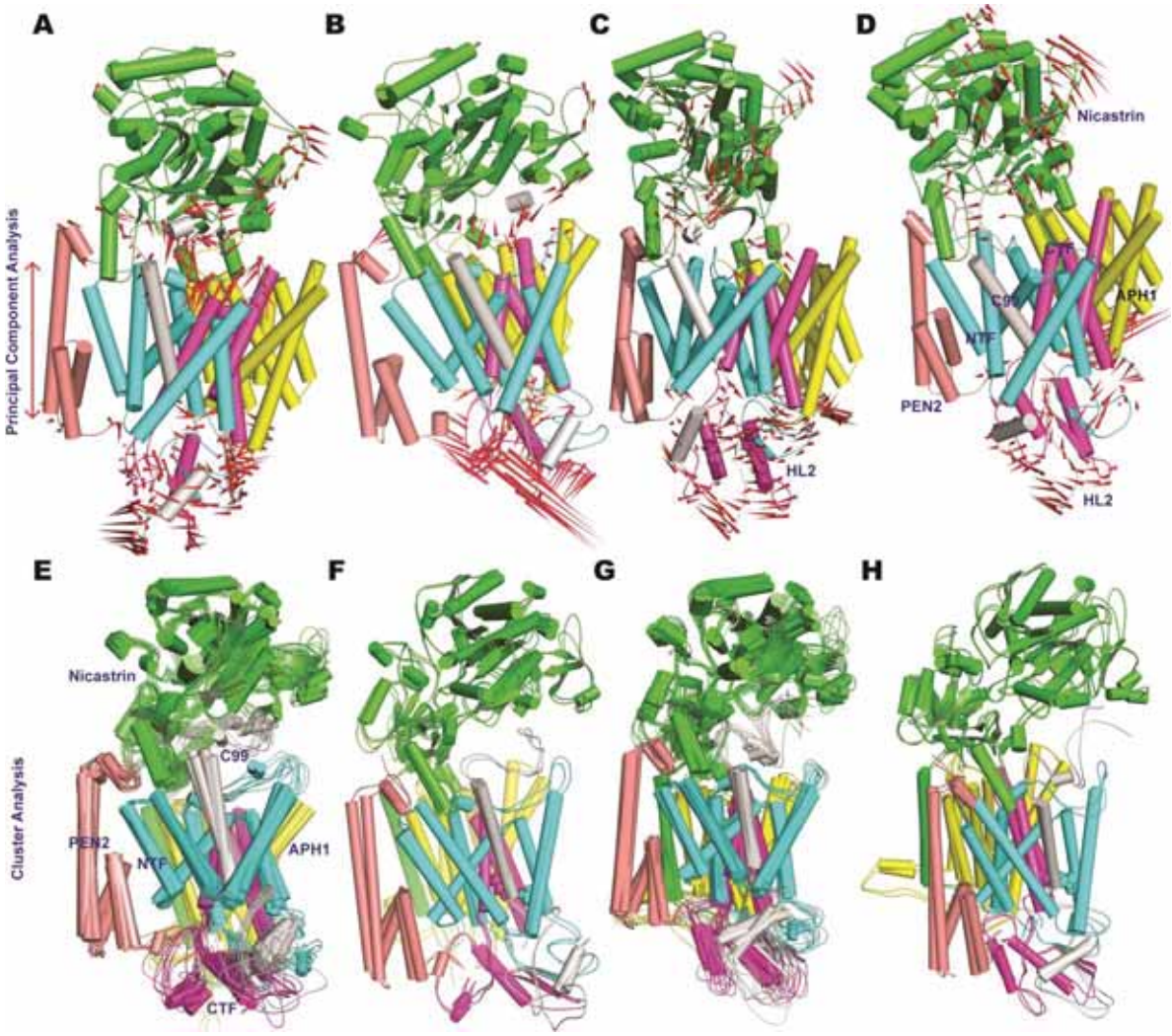

Figure 3. (A) Porcupine plot of eigenvector 1 motions from simulation 1. **(B)** Porcupine plot of eigenvector 2 motions from simulation 1. **(C)** Porcupine plot of eigenvector 1 motions from simulation 2. **(D)** Porcupine plot of eigenvector 2 motions from simulation 2. Red needles show the direction and amplitude of motions. **(E)-(H)** The structural superimposition of the representative top-ranked cluster structure (**E** and **G**) and top-two cluster (**F** and **H**) of C99-γ-secretase colored by different subunits (Green: Nicastrin, PS1 NTF: Cyan, PS1 CTF: Magenta, APH1: Yellow, PEN2: Wheat and C99: Light gray).

Essential dynamics of membrane-bound C99-γ-secretase

To understand the atomic contributions to the subunit dynamics in **Figure 2** in detail, we performed PCA to identify the most significant collective motions in the phase space,

emphasizing the first two eigenvectors (EV1 and EV2). **Figure 3A** and **3B** show EV1 and EV2 for simulation 1, whereas **Figure 3C** and **3D** show EV1 and EV2 for simulation 2. Structural motions in NCT-ECD occur both in the part of NCT that orients toward APH1 and in the part that interacts with PS1 and the membrane (top, green subunit). The latter motions affect atoms associated with the PS1-C99 complex consistent with a role of these NCT motions in substrate recognition[24]. PCA confirmed that the NCT-ECD interacts with HL1 of PS1 in and open-close movement, suggesting that it can affect substrate entry into the PS1 active site. Compared to the PCA of the apo-form of γ-secretase in this work (**Figure S6**) and previous MD simulation studies[76], the large C99 substrate restricts this movement somewhat via packing interactions with HL1; thus the bound state displays a somewhat dampened NCT motion relative to the apostate of the protein complex.

We also find that the large HL2 (as shown in **Figure 3C** and **3D**), which has been cleaved in our modeled mature state of the protein, displays a characteristic "left-right" and "in-out" movement, which can affect the translocation of the C99 to the catalytic center, but also water access, important because a water molecule is required as nucleophile in the active site, and membrane-channel-like morphology. As shown before, in the immature state, the HL2 is a plug in the active site, whereas auto-cleavage of the plug enables access to the active site in the mature protein complex[42]. Because of this maturation, the movements of HL2 are substantially more significant than those of HL1. Porcupine plots of PC1 and PC2 of the catalytic subunit PS1 (**Figure S7**) show strong inward-outward motions of HL2, whereas negligible movements occur for HL1. The significant motions of HL2 contribute to the strong fluctuations in the RMSF plot (**Figure 2**).

The two most representative snapshot structures for each simulation are shown in **Figure 3E-3H**. C99-bound γ-secretase is characterized by several conformational states, which in the case of PS1 even affects the secondary structure, which is unusual. The representative structures show

different packing of the TM helices of PS1 around C99 (cyan) resulting in differential compactness. In one state, C99 shows large dynamic interaction with NCT (gray, **Figure 3E**), which is elusive in the cryo-EM structure because the N-terminal of C99 is missing in C83. The residue-wise thermal fluctuation parameters in **Figure 2J** document these structural differences as well as a major conformational flexibility of C99 in its out-of-membrane loop interactions, bottom of **Figure 3**, which will probably be smaller at cryo-temperature.

We computed the intermolecular contacts between C99 and γ-secretase (**Table S3** and **S4**) from the two simulations. The number of inter-molecular hydrogen bonds formed between NCT and PS1 and C99 differed significantly between the two ensembles, such that one ensemble represents a more compact C99 state (simulation 2: **Figure 4**), and the other represents a distinctly looser C99 state (simulation 1) (**Figure S8** and **S9**). The compact conformation displayed the shortest average distance between interaction pairs and the most persistent C99-protein interactions, with the longest residence time of C99-γ-secretase interactions (**Figure 4**). Most residues of the C99-TMD (Gly29–Leu52), including the sites of ε-cleavage (Ala42), ζ-cleavage (Ile45), γ-cleavage (Thr48 and Leu49), and substrate recognition (Met51, Lys52) interact strongly with PS1 by hydrophobic interactions or hydrogen bonds. The triplet lysine anchor Lys53-Lys54-lys55 engages in direct salt bridges as well as persistent hydrogen bonding to PS1.

Assuming that longer residence time of C99-protein interactions correlates with the extent of cleavage of C99, our identified two states of C99 may explain the changes in the production of longer (loose state) vs. shorter (compact state) Aβ peptides in various forms of the protein. This possibility is substantiated below by calculations of the stability of the enzyme-substrate complexes and PS1 helix tilt angles relating directly to Asp-Asp distance.

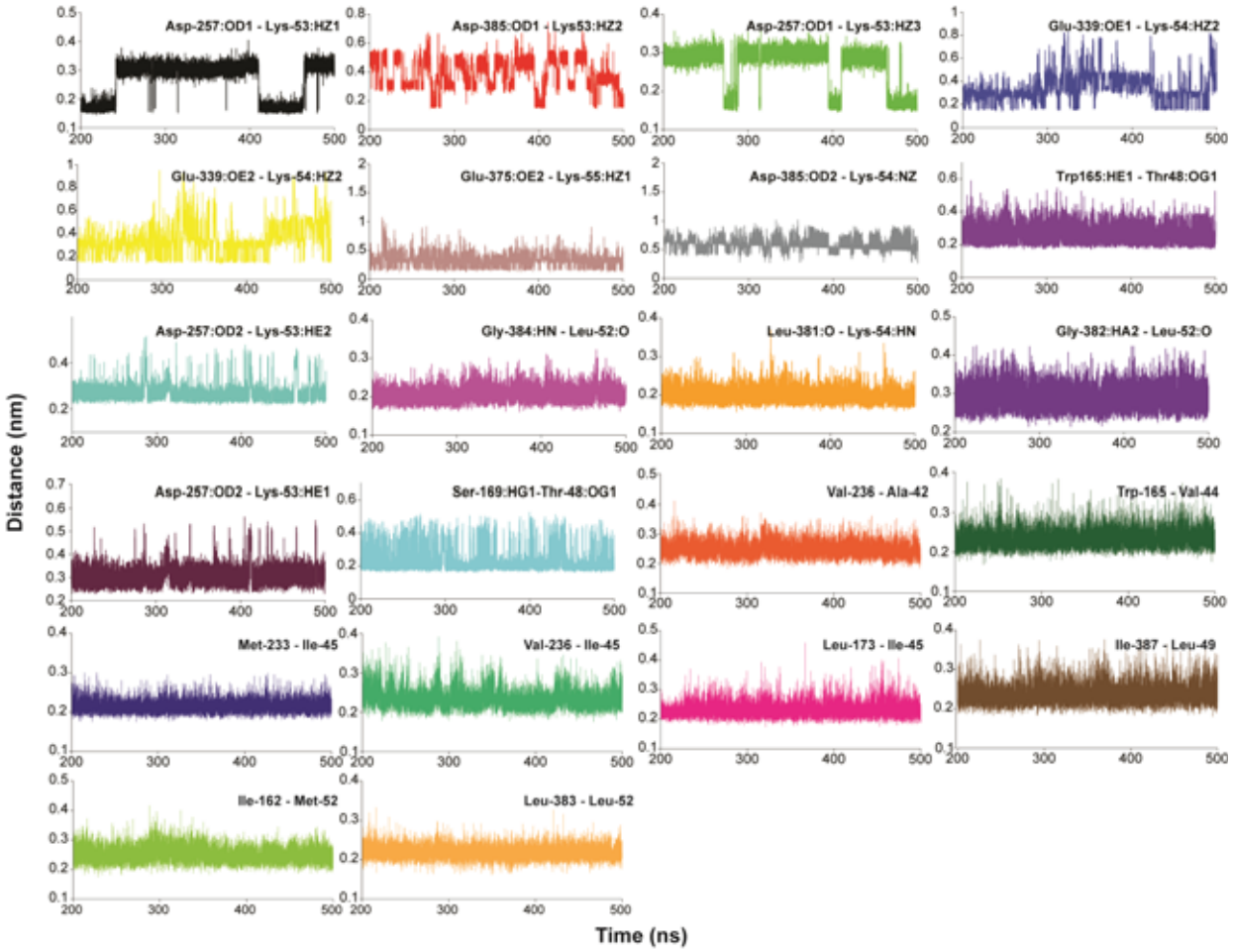

Figure 4. The minimum inter-atomic distance profile of key residues interacting with C99 in the compact ensemble (simulation 2, 200-500 ns).

PS1 helix tilt angles define C99 residence time

Recent MD simulations of γ-secretase indicate that the compactness of the substrate binding site and the distance between the catalytic aspartates (dd_{Asp}) in PS1 depend on the orientation of different TM helices[76]. The functionally important dd_{Asp} fluctuates around an average value of ~1 nm. To understand the helix translocations, which are known to be well-sampled on the applied timescale[34], we computed the distribution of TM tilt angles as shown in **Figure 5**. These angles effectively differentiate the various conformational states of PS1 in γ-secretase. TM2 displays a notable two-state behavior in simulation 1 (**Figure 5** top), associated with a weak two-state behavior of TM3 and a broader TM6 tilt angle distribution. Intriguingly these

three helices (TM2, TM3, and TM6) also display correlated motions in the apo-complex and lead to open, semi-open, and closed conformational states[30]. Whereas most helices are more compact in simulation 2, TM8 is flexible in both simulations and displays a clearly visible two-state dynamics in simulation 2. Thus, from a protein perspective, the C99-bound states display flexibility that resembles the apo-complex, with simulation 1 showing most of the variation in helix tilt angles.

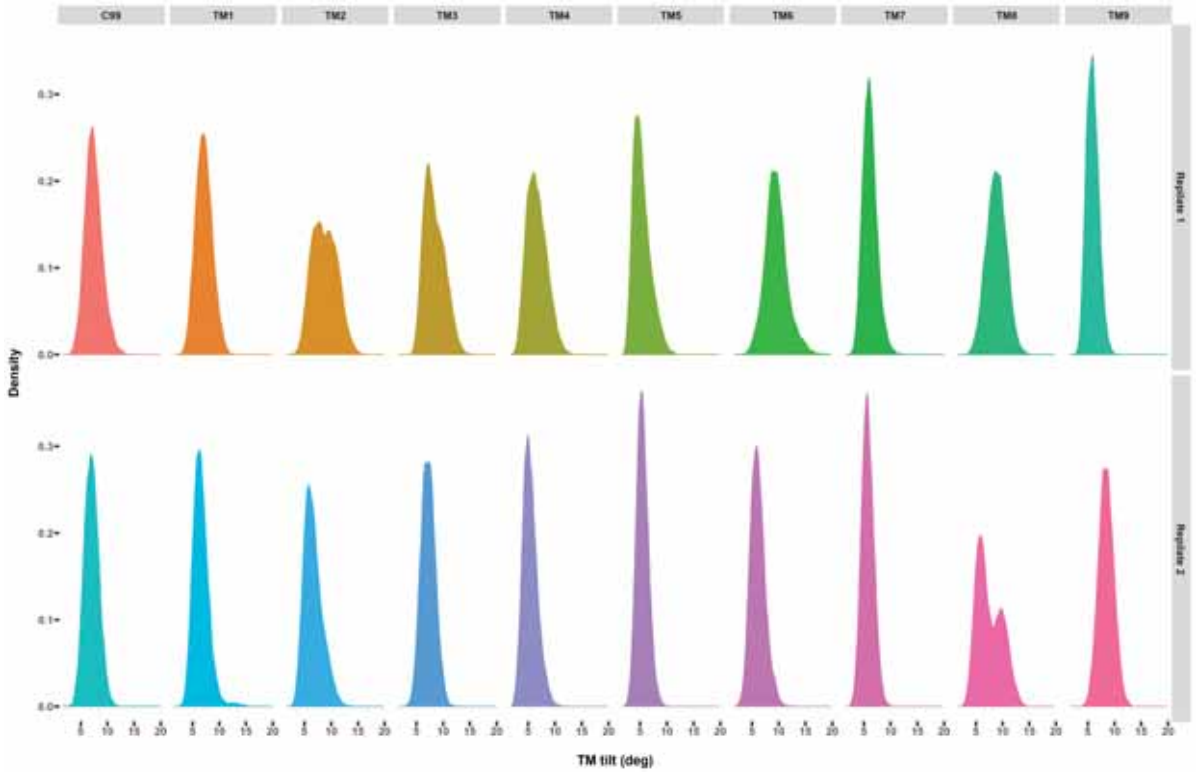

Figure 5. Distribution of tilt angles of the PS1 and C99 TMs calculated from the last 300 ns trajectory of the two replicates.

To understand the impact of these TM helix movements on the catalytically important dd_{Asp}, which potentially defines residence time and processing of C99, the simulated structural ensembles were projected onto the dd_{Asp} distance and tilt angles for all TMs in **Figure 6**. **Figures S10** and **S11** display the corresponding distributions of the dd_{Asp} distance and the tilt angles for

the apoform of γ-secretase, to understand the impact of C99 binding. Most importantly, both the apo-γ-secretase (**Figure S11**) and C99-bound γ-secretase (**Figure 6**) ensembles feature a loose and a distinctly more compact conformation state. For the loose apo-state, dd_{Asp} reaches 1.3 nm, whereas the compact state features dd_{Asp} in the range 0.9-1.1 nm. Once C99 is bound, dd_{Asp} of the loose state varies from 0.98-1.15 nm, while for the compact state is varies from 0.90-1.02 Å. These differences are highly significant and the opening correlates with changes mainly in TM2, TM6, and TM8 (**Figure 6 top**). Not only the variability but also the distribution of the tilt angles (horizontal axis in **Figure 6**) change. TM6 undergoes an important tilt angle modification, which strongly correlates with modulation of dd_{Asp}. In addition, changes in the tilt angles of TM2 and TM9 correlate with tilt angles of TM6 and TM7. Experimental studies have suggested that TM2 and TM9 contribute to the initial substrate-binding site in PS1 enabling C99 to enter either between TM6 and TM9 or between TM2 and TM6[67,77]. The higher flexibility of TM2 confirms its previously suggested role in the gate opening[30]. The wide tilt angle distribution of TM2 and TM9 affirms the high mobility of these helices seen in previous studies[27].

Distance measurement was performed between terminal Cα atoms as shown in **Figure S12**. In the loose state of simulation 1, all the TMs except TM3, TM7 TM9 and the TMD of C99 displayed higher fluctuation in distances. In contrast, the RMSD of TM3, TM7 and TM9 in the compact state demonstrated higher mobility (**Figure S13**), signifying that the substrate binding induces cooperative changes in the structure.

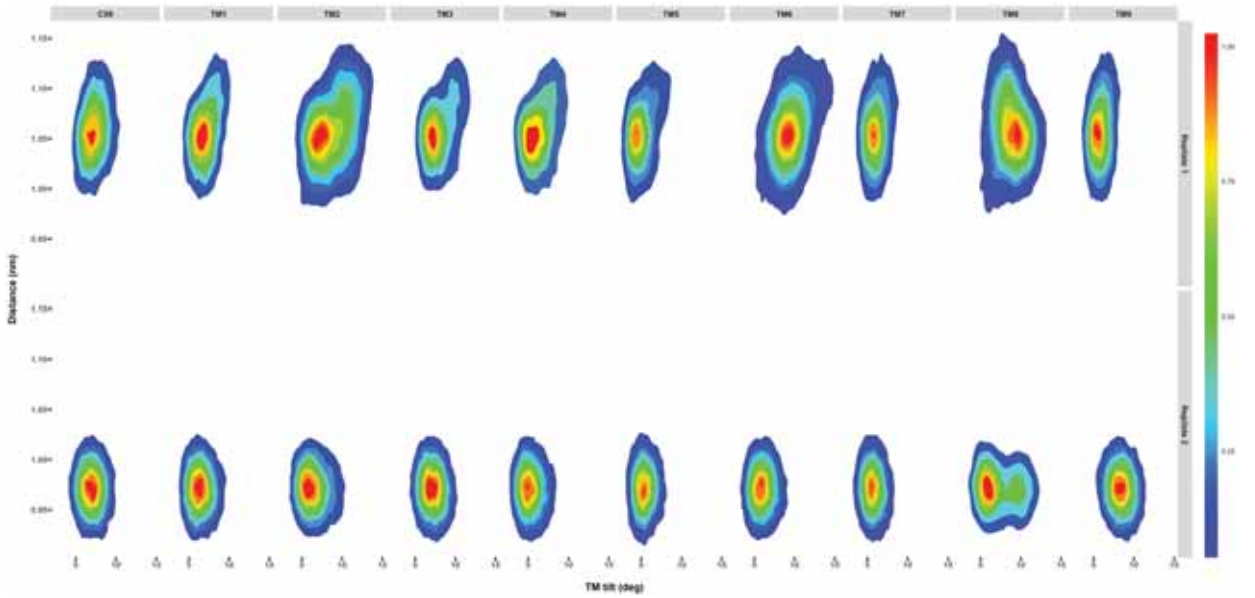

Figure 6. Distribution of snapshots projected onto the distance between the catalytic Asp-263 and Asp-366 and the tilt angle distribution of TMs during the last 300 ns of the two MD simulations of C99-γ-secretase. The colored scale defines the relative populations.

Atomic-resolution mechanism of C99 binding and processing within γ-secretase

After identifying two major conformation states of C99-γ-secretase, we explored the details and contributions of individual amino acids of both C99 and γ-secretase to these two states. To obtain the energy contribution of each residue to the total binding energy, MM/PBSA calculations were performed for 100 equidistant snapshots of the last 300 ns of each ensemble. This local binding energy obtained from such calculations relate to K_M, which represents the lifetime of the active poses of C99 leading to productive turnover. This is distinct from the total binding free energy (affinity) of C99 to the protein complex, which involves many other nonproductive conformation states. k_{cat} of γ-secretase is very small, of the order of 0.0012 s^{-1}[3], possibly due to the rate-limiting access of nucleophile water to the buried active site of C99-γ-secretase. K_M has been measured to be surprisingly large, 0.2 mM, for a substrate the size of C99[3], and thus the turnover number becomes extremely small, of the order of 6 s^{-1} M^{-1}, and

this suggests kinetic control of the cleavage products probably governed by a higher k_{cat} of the more loose state but a lower K_M of the more compact state.

The calculated energies of binding of C99 are summarized in **Table S4**. The absolute binding energies are meaningless since the entropy is not included, whereas the relative values indicate a significant (vs. the standard deviations of the 100 calculations across the ensemble) difference in binding energy of C99 for the two conformation states. We also computed the inter-molecular contacts and contribution of each residue of γ-secretase to the C99 binding energy (**Figure S14** and **S15**). The two simulations revealed slightly different energies of contributing residues, but the major contributing residues were generally identical. The salt bridges dominate the energetics of binding, not surprisingly, but will be greatly compensated by entropy and thus again, the scale of energies is not physically meaningful, only the qualitative contribution.

We note that the Lys53-Lys54-Lys55 anchor interacts with both the CTF and NTF of PS1, which has implications for the two cleavage pathways initiating at $A\beta_{49}$ and leading to $A\beta_{40}$ in one case, and initiating with $A\beta_{48}$ and leading to $A\beta_{42}$ in the other case. The electrostatic interactions which dominate the energetics of C99 binding control the exact positioning of Thr48 and Leu49 in the two ensembles. An important observation is that Thr48 (belonging to the ε-cleavage site) is involved in hydrogen bonding with PS1-NTF, whereas Leu49 is hydrophobic packed with Ile387 of PS1-CTF; thus maturation cleavage produces two fragments that interact with each of the sites required for initiation of cleavage in the two pathways leading to $A\beta_{49}$ and $A\beta_{48}$. With the catalytic aspartates positioned on each site of C99 with access to one of these two sites, our MD simulations directly provide an atomic resolution model of the processing of C99 along the two pathways. Since the C99 forms a TM helix in this part, the next accessible peptide bond after Thr48-Leu49 on one side or Leu49-Val50 on the other side occurs three amino acids down the sequence of C99, and the simple translocation of the C99 helix thus most likely occurs directly after the first cleavage, leading to $A\beta_{42}$ and $A\beta_{40}$, respectively.

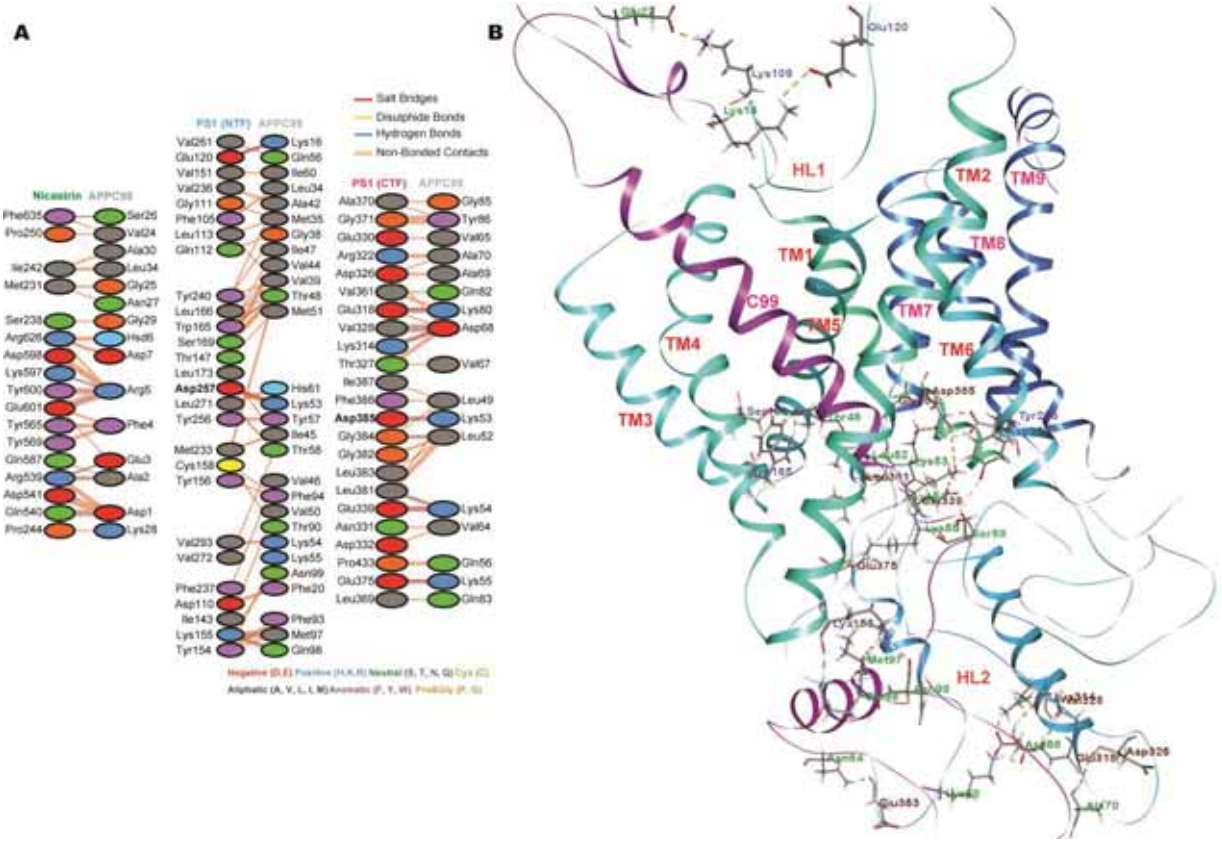

Figure 7. A) Inter-molecular contacts between NCT or PS1 (NTF and CTF) and C99 obtained from the top-ranked cluster of the compact ensemble of simulation 2. The catalytic Asp257 and Asp385 have been marked in bold. **B)** Line ribbon representation showing interaction of C99 (magenta) with NTF and CTF of PS1. Residues of C99 and PS1 forming hydrogen bonds and salt bridges are visualized in stick model. Yellow and green dotted lines represent the electrostatic and hydrogen bond interactions. The interacting residues of NTF are blue, those of CTF dark brown, and those of C99 green.

We also computed the minimum distance between the interacting atom pairs of the enzyme and substrate. From **Figure 7**, the interacting atom pairs of the compact C99-bound state displayed a strong and stable trend in distance, while the loose binding mode (simulation 1) displayed variable distances (**Figure S9**). We suggest that these two states

define the different processing of C99 leading to two trimming pathways and to longer or shorter Aβ peptides. The two fits of C99 may explain the experiment observation of two trimming pathways[6,78]. The loose conformation displays fewer interactions and is associated with shorter C99 residence time and by inference releases Aβ peptides of longer lengths.

Recent studies have shown two plausible binding sites of PS1: TM2, TM6 and TM9 form one site, and PS1-NTF, PEN2 and NCT ECD form the other site[67,79]. In addition, coarse-grained MD simulations suggest that C99-TMD can bind to the catalytic subunit (PS1) via TMD2/6/9[80]. We computed the intermolecular contacts of the top-ranked two structures obtained from clustering for both our simulations. We find that Met51 of C99-TMD forms crucial contacts with Ile149 and Met152 of TM2, while Val44 forms hydrophobic contacts with Leu166 (TM3). Furthermore, the key catalytic Asp257 (TM6) and Asp385 (TM7) form strong hydrogen bonds and salt bridges with the triplet Lysine anchor (Lys53-Lys54-Lys55 situated at the C-terminal end of C99-TMD), an indispensable element for substrate recognition[64] (**Figure 7** and **S9**). Recent studies[79,81] suggest that Val44, Leu49, Met51 and Leu52 residues of the C99-TMD act as the γ-secretase interaction sites, an observation that is supported and explained by our atomic resolution simulations. Also supporting our obtained ensembles, Xu et al.[63] recently showed that the conserved positively charge residues Lys53 in the C99-TMD crucially contributes to substrate recognition and cleavage. Mutational studies have confirmed the requirement of Lys53 within the C99-TMD and Notch (another major γ-secretase substrate), indicating that substrate recognition by γ-secretase is highly conserved. Our results show this role clearly but also indicate that not only Lys53 but also Lys54 and Lys55 contribute substantially to the substrate recognition *via* electrostatic interactions (**Figure 7 and S9**). In total, NTF of PS1 forms substantially more intermolecular contacts with C99 compared to CTF.

Since γ-secretase controls Aβ production it offers a primary therapeutic target for AD. The TM fragment of C83 is cleaved by γ-secretase to produce either $A\beta_{48}$ or $A\beta_{49}$; additional trimming releases $A\beta_{45/42/38}$ or $A\beta_{46/43/40}$[6,82]. Comparison of our C99-γ-secretase structure in the membrane to the new structure of C83-bound γ-secretase in frozen ice[19] suggest that the overall binding topology is very similar for C99 and C83 and with and without the membrane: NCT and HL1 interacts with the N-terminal of C99, and TM6 and TM7 of PS1 change conformation during binding, as compared both to previous apo-γ-secretase simulations in the membrane, and corresponding experimental cryo-EM data without the membrane.

The new structure of C83[19] suggests that the TM helix of C83 is partially unwound once bound, which could aid intramembrane proteolysis, and the substrate forms both a helix and a β-strand segment (**Figure S16A**). The unwinding plausibly exposes the peptide bonds to cleavage either at Thr719-Leu720 (resulting in $A\beta_{48}$) or at Leu720-Val721 (yielding $A\beta_{49}$). In our simulations, we observed loss of helicity of the C99-TMD (**Figure S17**), which supports that a helix unwinding also occurs in the membrane. The susceptibility of C83 to sequential trimming may be due to the presence of several helix-destabilizing residues in its TM that promote helix unwinding, rationalized by our data in **Figure S17**.

A specific feature of the new cryo-EM structure is a 3-stranded hybrid β-sheet comprised of two β-strands of PS1 (in the cytoplasmic HL2) and one from C83 (Met722-Lys725) (**Figure S16B, S16C**). It is interesting to know whether the membrane and C83/C99 difference changes this tendency. In the cryo-EM structure, the induced β-strand of C83 interacts with the PAL motif, which in turn stabilizes the C83 β-strand. In our structures produced before publication of the new C83 structure, we observed two β-strands (Lys286-Ser290 and Thr327-Asn331) in HL2. The unusual propensity for strand formation in PS1 was first observed by MD simulation in 2016, although not discussed in that paper[42]. In our

simulations C99 did not form any β-strand (**Figure S16B**) and thus we do not observe a substrate-PS1 β-sheet recognition motif. C83 binds substantially more strongly than C99 and may thus induce structure not seen for C99, or cryo temperature could plausibly stabilize it. Alternatively, our MD simulations may be inaccurate on this detail. Regardless of the answer, it is evident from what is now known that HL2 has major secondary-structure variability that is important both for autocleavage (requiring helix in the loop when it becomes substrate) and substrate recognition.

We suggest that the extent of C99 trimming depends on the relative prevalence (as determined by the relative free energy) of the compact and loose conformation states identified in our work. This balance could easily be affected by binding small molecules or by mutation. The loose state is associated with less favorable interactions with the catalytic site and reduced residence time of important interactions, and this will plausibly reduce the extent of C99 trimming. These findings are in accordance with the FIST model (Fit-Stay-Trim) of C99 processing[42,43]. They are also supported by the observation that $A\beta_{42}/A\beta_{40}$ ratios of FAD-causing PSEN1 mutations correlate with disease severity[44], and both of these correlate with the tendency of the mutation to chemically stabilize the hydrophobic packing of the protein complex within the membrane, with PSEN1 mutations generally loosing thermochemical stability and/or hydrophobicity[83].

Conclusions

γ-secretase, an important intramembrane-cleaving aspartyl protease, is responsible for cleaving C99 into the Aβ peptides central to AD, with longer Aβ peptides being more aggregation-prone and toxic and enriched in senile plaques of AD patients. The molecular processing of C99, well-known from cell assays, has missed a structural basis until the new cryo-EM structure of C83 in frozen ice[19]. Translocation of the substrate to the active site is known from previous studies to involve major conformational changes of the γ-secretase complex[32,69,77]. A recent study[79] demonstrated that C99 binds first to NCT and PEN2 and then subsequently binds PS1-NTF and the active site.

Our all-atom molecular dynamics simulations describe the probable modes of binding of full-length C99 to mature γ-secretase in a pure lipid bilayer at ambient temperature and thus substantially complements the new cryo-EM structure of C83-γ-secretase. The model obeys all relevant experimental constraints and was subject to extensive quality control, with its topology in excellent agreement with known direct (electron microscopy) and indirect (assaying and site-directed mutagenesis) data. Our study reveals that the weaker binding of C99 vs. C83 induces variability in the binding mode and produces two major binding modes of C99 which differ in compactness, stability, and retention time near the catalytic aspartates. The open state features longer catalytic Asp-Asp distance correlating with changes in TM2, TM6, and TM9. Both states are in equilibrium and suggest that the longer substrate retention and tighter intermolecular binding in the compact state leads to maximum trimming of C99 and thus shorter Aβ peptides. FAD PS1 mutations shift the equilibrium in favor of the loose ensemble to a variable extent.

We find that the GxxG motif of the N-terminal of C99 contribute consistently to the packing of C99 within γ-secretase. Supporting recent observations by Yan et al.[64] the triplet lysine anchor (Lys53-Lys54-Lys55) substantially contributes to C99 binding. We show

that this occurs in a cavity formed primarily by TM2, TM3, and TM5, with movements in TM6 controlling precision and compactness of C99 binding, particularly near the hydrophobic cleavage sites at Thr48 and Leu49. Very interestingly, Thr48 interacts predominantly with PS1-NTF as most C99 residues do, whereas Leu-49 interacts mainly with the CTF of PS1, directly indicating how maturation cleavage enhances flexibility that affects C99 positioning. Since the two catalytic aspartates are positioned on each side of C99 close to either Thr48 or Leu49, the data suggest that the exact positioning of the aspartates relative to the Thr48-Leu49 and Leu49-Val50 peptide bonds defines the two cleavage pathways initiating with production of $A\beta_{49}$ and $A\beta_{48}$. We show that the looser state (**Figure 6** top) features a more dynamic C99, longer dd_{Asp} and accommodates more of both cleavage pathways, whereas the compact state (**Figure 6** bottom) favors cleavage at Thr48-Leu49 to form the innocent $A\beta_{40}$. These two states cannot be directly seen in the cryo-EM data as they average out. The free energy balance between the compact and loose ensembles defines the extent of trimming, which is primarily determined by the reduced enzyme-complex stability as trimming proceeds[84]. We thus hope to have identified the molecular mechanism at atomic resolution that explains Aβ production.

Our molecular structures and dynamics will aid the development of new medicine for the treatment of AD with a structural causal basis. Specifically, new γ-secretase modulators should enhance the processing of C99 by favoring the ensemble of the compact state over the loose state that we have identified in this work. Such compounds would contribute their binding energy to the ternary complex to increase residence time of C99, and accordingly increasing proteolytic trimming towards shorter non-toxic Aβ peptides. Further mechanistic and structural studies are needed to address the dynamics of the system in different biophysical environments, as our study only details the most important qualitative properties of the ensemble, with quantitative insights being most likely context-dependent.

Conflict of Interest

The authors declare no conflict of interest.

Supporting Information

The supplementary information pdf file contains details on the atomic model building, MD simulations, C99-protein interactions, and additional analysis of the ensembles. The file clusters.rar includes the two representative structures of the full equilibrated system from simulation 1 and 2, respectively.

Author contributions

BD performed most calculations and analysis, and wrote the first draft of the paper. KPK planned the project, analyzed results and wrote the paper with BD. NT contributed analysis of helix tilt angles and trajectory and statistical analysis.

Acknowledgements

The authors acknowledge the financial support received from the Novo Nordisk Foundation, grant NNF17OC0028860, and the Danish Council for Independent Research | Natural Sciences (DFF), grant 7016-00079B. We acknowledge computer resources from the High-Performance-Computing facility of Technical University of Denmark (DTU).

References

1 Kimberly, W. T., LaVoie, M. J., Ostaszewski, B. L., Ye, W., Wolfe, M. S. and Selkoe, D. J. (2003) Gamma-secretase is a membrane protein complex comprised of presenilin, nicastrin, Aph-1, and Pen-2. Proc. Natl. Acad. Sci. **100**, 6382–6387.

2 Haass, C., Kaether, C., Thinakaran, G. and Sisodia, S. (2012) Trafficking and proteolytic processing of APP. Cold Spring Harb. Perspect. Med. **2**, a006270.

3 Kamp, F., Winkler, E., Trambauer, J., Ebke, A., Fluhrer, R. and Steiner, H. (2015) Intramembrane proteolysis of β-amyloid precursor protein by γ-secretase is an unusually slow process. Biophys. J. **108**, 1229–1237.

4 Tomita, T. (2014) Molecular mechanism of intramembrane proteolysis by γ-secretase. J. Biochem. **156**, 195–201.

5 Zhang, H., Ma, Q., Zhang, Y. W. and Xu, H. (2012) Proteolytic processing of Alzheimer's β-amyloid precursor protein. J. Neurochem. **120**, 9–21.

6 Fukumori, A., Fluhrer, R., Steiner, H. and Haass, C. (2010) Three-amino acid spacing of presenilin endoproteolysis suggests a general stepwise cleavage of gamma-secretase-mediated intramembrane proteolysis. J. Neurosci. **30**, 7853–7862.

7 Zoltowska, K. M., Maesako, M. and Berezovska, O. (2016) Interrelationship between Changes in the Amyloid β 42/40 Ratio and Presenilin 1 Conformation. Mol. Med. **22**, 329–337.

8 Hsiao, K., Chapman, P., Nilsen, S., Eckman, C., Harigaya, Y., Younkin, S., Yang, F. and Cole, G. (1996) Correlative memory deficits, Aβ elevation, and amyloid plaques in transgenic mice. Science **274**, 99–102.

9 Duering, M., Grimm, M. O. W., Grimm, H. S., Schroder, J. and Hartmann, T. (2005) Mean age of onset in familial Alzheimer's disease is determined by amyloid beta 42. Neurobiol. Aging **26**, 785–788.

10 Oehlrich, D., Berthelot, D. J.-C. and Gijsen, H. J. M. (2010) γ-Secretase Modulators as Potential Disease Modifying Anti-Alzheimer's Drugs. J. Med. Chem. **54**, 669–698.

11 Golde, T. E., Koo, E. H., Felsenstein, K. M., Osborne, B. A. and Miele, L. (2013) γ-Secretase inhibitors and modulators. Biochim. Biophys. Acta - Biomembr. **1828**, 2898–2907.

12 Pester, O., Barrett, P. J., Hornburg, D., Hornburg, P., Pröbstle, R., Widmaier, S., Kutzner, C., Dürrbaum, M., Kapurniotu, A., Sanders, C. R., et al. (2013) The backbone dynamics of the amyloid precursor protein transmembrane helix provides a rationale for the sequential cleavage mechanism of γ-secretase. J. Am. Chem. Soc. **135**, 1317–1329.

13 Dominguez, L., Meredith, S. C., Straub, J. E. and Thirumalai, D. (2014) Transmembrane fragment structures of amyloid precursor protein depend on membrane surface curvature. J. Am. Chem. Soc. **136**, 854–857.

14 Pantelopulos, G. A., Straub, J. E., Thirumalai, D. and Sugita, Y. (2018) Structure of APP-C991–99 and implications for role of extra-membrane domains in function and oligomerization. Biochim. Biophys. Acta - Biomembr. **1860**, 1698–1708.

15 Barrett, P. J., Song, Y., Van Horn, W. D., Hustedt, E. J., Schafer, J. M., Hadziselimovic, A., Beel, A. J. and Sanders, C. R. (2012) The amyloid precursor protein has a flexible transmembrane domain and binds cholesterol. Science **336**, 1168–1171.

16 Kukar, T. L., Ladd, T. B., Robertson, P., Pintchovski, S. A., Moore, B., Bann, M. A., Ren, Z., Jansen-West, K., Malphrus, K., Eggert, S., et al. (2011) Lysine 624 of the amyloid precursor protein (APP) is a critical determinant of amyloid β peptide length: Support for a sequential model of γ-secretase intramembrane proteolysis and regulation by the amyloid β precursor protein (APP) juxtamembrane region. J. Biol.

Chem. **286**, 39804–39812.

17 Zhou, L., Brouwers, N., Benilova, I., Vandersteen, A., Mercken, M., Van Laere, K., Van Damme, P., Demedts, D., Van Leuven, F., Sleegers, K., et al. (2011) Amyloid precursor protein mutation E682K at the alternative β-secretase cleavage β'-site increases Aβ generation. EMBO Mol. Med. **3**, 291–302.

18 Dimitrov, M., Alattia, J.-R., Lemmin, T., Lehal, R., Fligier, A., Houacine, J., Hussain, I., Radtke, F., Dal Peraro, M., Beher, D., et al. (2013) Alzheimer's disease mutations in APP but not γ-secretase modulators affect epsilon-cleavage-dependent AICD production. Nat. Commun. **4**, 2246.

19 Zhou, R., Yang, G., Guo, X., Zhou, Q., Lei, J. and Shi, Y. (2019) Recognition of the amyloid precursor protein by human γ-secretase. Science **363**, eaaw0930.

20 De Strooper, B. (2003) Aph-1, Pen-2, and Nicastrin with Presenilin generate an active γ-Secretase complex. Neuron **38**, 9–12.

21 Haapasalo, A. and Kovacs, D. M. (2011) The many substrates of presenilin/γ-secretase. J. Alzheimer's Dis. **25**, 3–28.

22 De Strooper, B., Iwatsubo, T. and Wolfe, M. S. (2012) Presenilins and γ-secretase: structure, function, and role in Alzheimer Disease. Cold Spring Harb. Perspect. Med. **2**, a006304.

23 Francis, R., McGrath, G., Zhang, J., Ruddy, D. A., Sym, M., Apfeld, J., Nicoll, M., Maxwell, M., Hai, B., Ellis, M. C., et al. (2002) aph-1 and pen-2 are required for Notch pathway signaling, γ-secretase cleavage of βAPP, and presenilin protein accumulation. Dev. Cell **3**, 85–97.

24 Bolduc, D. M., Montagna, D. R., Gu, Y., Selkoe, D. J. and Wolfe, M. S. (2016) Nicastrin functions to sterically hinder γ-secretase–substrate interactions driven by substrate transmembrane domain. Proc. Natl. Acad. Sci. USA **113**, E509–E518.

25 Lu, P., Bai, X., Ma, D., Xie, T., Yan, C., Sun, L., Yang, G., Zhao, Y., Zhou, R., Scheres, S. H. W., et al. (2014) Three-dimensional structure of human γ-secretase. Nature **512**, 166–170.

26 Sun, L., Zhao, L., Yang, G., Yan, C., Zhou, R., Zhou, X., Xie, T., Zhao, Y., Wu, S., Li, X., et al. (2015) Structural basis of human γ-secretase assembly. Proc. Natl. Acad. Sci. USA. **112**, 6003–6008.

27 Bai, X., Yan, C., Yang, G., Lu, P., Sun, L., Zhou, R., Scheres, S. H. W. and Shi, Y. (2015) An atomic structure of human γ-secretase. Nature **525**, 212–218.

28 Bai, X., Rajendra, E., Yang, G., Shi, Y. and Scheres, S. H. (2015) Sampling the conformational space of the catalytic subunit of human γ-secretase. Elife **4**, 551–560.

29 Yang, G., Zhou, R., Zhou, Q., Guo, X., Yan, C., Ke, M., Lei, J. and Shi, Y. (2019) Structural basis of Notch recognition by human γ-secretase. Nature **565**, 192–197.

30 Somavarapu, A. K. and Kepp, K. P. (2017) Membrane Dynamics of γ-Secretase Provides a Molecular Basis for β-Amyloid Binding and Processing. ACS Chem. Neurosci. **8**, 2424–2436.

31 Tolia, A., Horré, K. and De Strooper, B. (2008) Transmembrane domain 9 of presenilin determines the dynamic conformation of the catalytic site of γ-secretase. J. Biol. Chem. **283**, 19793–19803.

32 Elad, N., De Strooper, B., Lismont, S., Hagen, W., Veugelen, S., Arimon, M., Horré, K., Berezovska, O., Sachse, C. and Chávez-Gutiérrez, L. (2015) The dynamic conformational landscape of γ-secretase. J. Cell Sci. **128**, 589–598.

33 Karplus, M. and McCammon, J. A. (2002) Molecular dynamics simulations of biomolecules. Nat. Struct. Biol. **9**, 646–652.

34 Adcock, S. A. and McCammon, J. A. (2006) Molecular dynamics: survey of methods for simulating the activity of proteins. Chem. Rev. **106**, 1589–1615.

35 Zwier, M. C. and Chong, L. T. (2010) Reaching biological timescales with all-atom molecular dynamics simulations. Curr. Opin. Pharmacol. **10**, 745–752.

36 Best, R. B., Buchete, N.-V. and Hummer, G. (2008) Are current molecular dynamics force fields too helical? Biophys. J. **95**, L07–L09.

37 Somavarapu, A. K. and Kepp, K. P. (2015) The Dependence of Amyloid-β Dynamics on Protein Force Fields and Water Models. ChemPhysChem **16**, 3278–3289.

38 Lindorff-Larsen, K., Maragakis, P., Piana, S., Eastwood, M. P., Dror, R. O. and Shaw, D. E. (2012) Systematic validation of protein force fields against experimental data. PLoS One **7**, 1–6.

39 Miyashita, N., Straub, J. E., Thirumalai, D. and Sugita, Y. (2009) Transmembrane structures of amyloid precursor protein dimer predicted by replica-exchange molecular dynamics simulations. J. Am. Chem. Soc. **131**, 3438–3439.

40 Dominguez, L., Foster, L., Straub, J. E. and Thirumalai, D. (2016) Impact of membrane lipid composition on the structure and stability of the transmembrane domain of amyloid precursor protein. Proc. Natl. Acad. Sci. **113**, E5281–E5287.

41 Meckler, X. and Checler, F. (2016) Presenilin 1 and presenilin 2 target γ-secretase complexes to distinct cellular compartments. J. Biol. Chem. **291**, 12821–12837.

42 Somavarapu, A. K. and Kepp, K. P. (2016) The dynamic mechanism of presenilin-1 function: Sensitive gate dynamics and loop unplugging control protein access. Neurobiol. Dis. **89**, 147–156.

43 Tang, N., Somavarapu, A. K. and Kepp, K. P. (2018) Molecular Recipe for γ-Secretase Modulation from Computational Analysis of 60 Active Compounds. ACS Omega **3**, 18078–18088.

44 Tang, N. and Kepp, K. P. (2018) Aβ42/Aβ40 ratios of presenilin 1 mutations correlate with clinical onset of Alzheimer's disease. J. Alzheimers Dis. **66**, 939–945.

45 Knappenberger, K. S., Tian, G., Ye, X., Sobotka-Briner, C., Ghanekar, S. V, Greenberg, B. D. and Scott, C. W. (2004) Mechanism of gamma-secretase cleavage activation: is gamma-secretase regulated through autoinhibition involving the presenilin-1 exon 9 loop? Biochemistry **43**, 6208–18.

46 Thinakaran, G., Borchelt, D. R., Lee, M. K., Slunt, H. H., Spitzer, L., Kim, G., Ratovitsky, T., Davenport, F., Nordstedt, C., Seeger, M., et al. (1996) Endoproteolysis of presenilin 1 and accumulation of processed derivatives in vivo. Neuron **17**, 181–90.

47 Shen, Y., Delaglio, F., Cornilescu, G. and Bax, A. (2009) TALOS+: A hybrid method for predicting protein backbone torsion angles from NMR chemical shifts. J. Biomol. NMR **44**, 213–223.

48 Beel, A. J., Mobley, C. K., Kim, H. J., Tian, F., Hadziselimovic, A., Jap, B., Prestegard, J. H. and Sanders, C. R. (2008) Structural studies of the transmembrane C-terminal domain of the amyloid precursor protein (APP): does APP function as a cholesterol sensor? Biochemistry **47**, 9428–9446.

49 Pettersen, E. F., Goddard, T. D., Huang, C. C., Couch, G. S., Greenblatt, D. M., Meng, E. C. and Ferrin, T. E. (2004) UCSF Chimera - A visualization system for exploratory research and analysis. J. Comput. Chem. **25**, 1605–1612.

50 Hekkelman, M. L., te Beek, T. A. H., Pettifer, S. R., Thorne, D., Attwood, T. K. and Vriend, G. (2010) WIWS: A protein structure bioinformatics web service collection. Nucleic Acids Res. **38**, 719–723.

51 Kozakov, D., Hall, D. R., Xia, B., Porter, K. A., Padhorny, D., Yueh, C., Beglov, D. and Vajda, S. (2017) The ClusPro web server for protein-protein docking. Nat. Protoc. **12**, 255–278.

52 Lomize, M. A., Pogozheva, I. D., Joo, H., Mosberg, H. I. and Lomize, A. L. (2012) OPM database and PPM web server: resources for positioning of proteins in

membranes. Nucleic Acids Res. **40**, D370–D376.

53 Jo, S., Kim, T., Iyer, V. G. and Im, W. (2008) CHARMM-GUI: A web-based grraphical user interface for CHARMM. J. Comput. Chem. **29**, 1859–1865.

54 Jorgensen, W. L., Chandrasekhar, J., Madura, J. D., Impey, R. W. and Klein, M. L. (1983) Comparison of simple potential functions for simulating liquid water. J. Chem. Phys. **79**, 926.

55 Huang, J., Rauscher, S., Nawrocki, G., Ran, T., Feig, M., De Groot, B. L., Grubmüller, H. and MacKerell, A. D. (2016) CHARMM36m: An improved force field for folded and intrinsically disordered proteins. Nat. Methods **14**, 71–73.

56 Abraham, M. J., Murtola, T., Schulz, R., Páll, S., Smith, J. C., Hess, B. and Lindah, E. (2015) Gromacs: High performance molecular simulations through multi-level parallelism from laptops to supercomputers. SoftwareX **1**–**2**, 19–25.

57 Hess, B., Bekker, H., Berendsen, H. J. C. and Fraaije, J. G. E. M. (1997) LINCS: A Linear Constraint Solver for molecular simulations. J. Comput. Chem. **18**, 1463–1472.

58 Buchoux, S. (2017) FATSLiM: A fast and robust software to analyze MD simulations of membranes. Bioinformatics **33**, 133–134.

59 Daura, X., Gademann, K., Jaun, B., Seebach, D., Van Gunsteren, W. F. and Mark, A. E. (1999) Peptide Folding: When Simulation Meets Experiment. Angew. Chemie Int. Ed. **38**, 236–240.

60 Humphrey, W., Dalke, A. and Schulten, K. (1996) VMD: visual molecular dynamics. J. Mol. Graph. **14**, 33–38.

61 Kumari, R., Kumar, R. and Lynn, A. (2014) G-mmpbsa -A GROMACS tool for high-throughput MM-PBSA calculations. J. Chem. Inf. Model. **54**, 1951–1962.

62 Kollman, P. A., Massova, I., Reyes, C., Kuhn, B., Huo, S., Chong, L., Lee, M., Lee, T., Duan, Y., Wang, W., et al. (2000) Calculating structures and free energies of

complex molecules: Combining molecular mechanics and continuum models. Acc. Chem. Res. **33**, 889–897.

63 Xu, T. H., Yan, Y., Kang, Y., Jiang, Y., Melcher, K. and Xu, H. E. (2016) Alzheimer's disease-associated mutations increase amyloid precursor protein resistance to γ-secretase cleavage and the Aβ42/Aβ40 ratio. Cell Discov. **2**, 16026.

64 Yan, Y., Xu, T. H., Melcher, K. and Xu, H. E. (2017) Defining the minimum substrate and charge recognition model of gamma-secretase. Acta Pharmacol. Sin. **38**, 1412–1424.

65 Zhuang, X., Dávila-Contreras, E. M., Beaven, A. H., Im, W. and Klauda, J. B. (2016) An extensive simulation study of lipid bilayer properties with different head groups, acyl chain lengths, and chain saturations. Biochim. Biophys. Acta - Biomembr. **1858**, 3093–3104.

66 Klauda, J. B., Venable, R. M., Freites, J. A., O'Connor, J. W., Tobias, D. J., Mondragon-Ramirez, C., Vorobyov, I., MacKerell, A. D. and Pastor, R. W. (2010) Update of the CHARMM All-Atom Additive Force Field for Lipids: Validation on Six Lipid Types. J. Phys. Chem. B. **114**, 7830–7843.

67 Watanabe, N., Takagi, S., Tominaga, A., Tomita, T. and Iwatsubo, T. (2010) Functional analysis of the transmembrane domains of presenilin 1: Participation of transmembrane domains 2 and 6 in the formation of initial substrate-binding site of γ-secretase. J. Biol. Chem. **285**, 19738–19746.

68 Takagi-Niidome, S., Sasaki, T., Osawa, S., Sato, T., Morishima, K., Cai, T., Iwatsubo, T. and Tomita, T. (2015) Cooperative Roles of Hydrophilic Loop 1 and the C-Terminus of Presenilin 1 in the Substrate-Gating Mechanism of γ-Secretase. J. Neurosci. **35**, 2646–2656.

69 Tominaga, A., Cai, T., Takagi-Niidome, S., Iwatsubo, T. and Tomita, T. (2016)

Conformational Changes in Transmembrane Domain 4 of Presenilin 1 Are Associated with Altered Amyloid- 42 Production. J. Neurosci. **36**, 1362–1372.

70 Li, C. D., Xu, Q., Gu, R. X., Qu, J. and Wei, D. Q. (2017) The dynamic binding of cholesterol to the multiple sites of C99: As revealed by coarse-grained and all-atom simulations. Phys. Chem. Chem. Phys. **19**, 3845–3856.

71 Lemmin, T., Dimitrov, M., Fraering, P. C. and Dal Peraro, M. (2014) Perturbations of the straight transmembrane α-helical structure of the amyloid precursor protein affect its processing by γ-secretase. J. Biol. Chem. **289**, 6763–6774.

72 Tian, G., Sobotka-Briner, C. D., Zysk, J., Liu, X., Birr, C., Sylvester, M. A., Edwards, P. D., Scott, C. D. and Greenberg, B. D. (2002) Linear non-competitive inhibition of solubilized human γ-secretase by pepstatin A methylester, L685458, sulfonamides, and benzodiazepines. J. Biol. Chem. **277**, 31499–31505.

73 Scharnagl, C., Pester, O., Hornburg, P., Hornburg, D., Götz, A. and Langosch, D. (2014) Side-chain to main-chain hydrogen bonding controls the intrinsic backbone dynamics of the amyloid precursor protein transmembrane helix. Biophys. J. **106**, 1318–1326.

74 Oestereich, F., Bittner, H. J., Weise, C., Grohmann, L., Janke, L.-K., Hildebrand, P. W., Multhaup, G. and Munter, L.-M. (2015) Impact of Amyloid Precursor Protein Hydrophilic Transmembrane Residues on Amyloid-Beta Generation. Biochemistry **54**, 2777–2784.

75 Langosch, D. and Steiner, H. (2017) Substrate processing in intramembrane proteolysis by γ-secretase-the role of protein dynamics. Biol. Chem. **398**, 441–453.

76 Aguayo-Ortiz, R., Chávez-García, C., Straub, J. E. and Dominguez, L. (2017) Characterizing the structural ensemble of γ-secretase using a multiscale molecular dynamics approach. Chem. Sci. **8**, 5576–5584.

77 Kornilova, A. Y., Bihel, F., Das, C. and Wolfe, M. S. (2005) The initial substrate-binding site of -secretase is located on presenilin near the active site. Proc. Natl. Acad. Sci. **102**, 3230–3235.

78 Takami, M., Nagashima, Y., Sano, Y., Ishihara, S., Morishima-Kawashima, M., Funamoto, S. and Ihara, Y. (2009) γ-Secretase: successive tripeptide and tetrapeptide release from the transmembrane domain of β-carboxyl terminal fragment. J. Neurosci. **29**, 13042–13052.

79 Fukumori, A. and Steiner, H. (2016) Substrate recruitment of γ-secretase and mechanism of clinical presenilin mutations revealed by photoaffinity mapping. EMBO J., e201694151.

80 Li, S., Zhang, W. and Han, W. (2017) Initial Substrate Binding of γ-Secretase: The Role of Substrate Flexibility. ACS Chem. Neurosci. **8**, 1279–1290.

81 Steiner, H., Fukumori, A., Tagami, S. and Okochi, M. (2018) Making the final cut: pathogenic amyloid-β peptide generation by γ-secretase. Cell Stress **2**, 292–310.

82 Quintero-Monzon, O., Martin, M. M., Fernandez, M. A., Cappello, C. A., Krzysiak, A. J., Osenkowski, P. and Wolfe, M. S. (2011) Dissociation between the processivity and total activity of γ-secretase: Implications for the mechanism of Alzheimer's disease-causing presenilin mutations. Biochemistry **50**, 9023–9035.

83 Somavarapu, A. K. and Kepp, K. P. (2016) Loss of stability and hydrophobicity of presenilin 1 mutations causing Alzheimer's Disease. J. Neurochem. **137**, 101–111.

84 Szaruga, M., Munteanu, B., Lismont, S., Veugelen, S., Horré, K., Mercken, M., Saido, T. C., Ryan, N. S., De Vos, T., Savvides, S. N., et al. (2017) Alzheimer's-Causing Mutations Shift Aβ Length by Destabilizing γ-Secretase-Aβn Interactions. Cell **170**, 443–456.

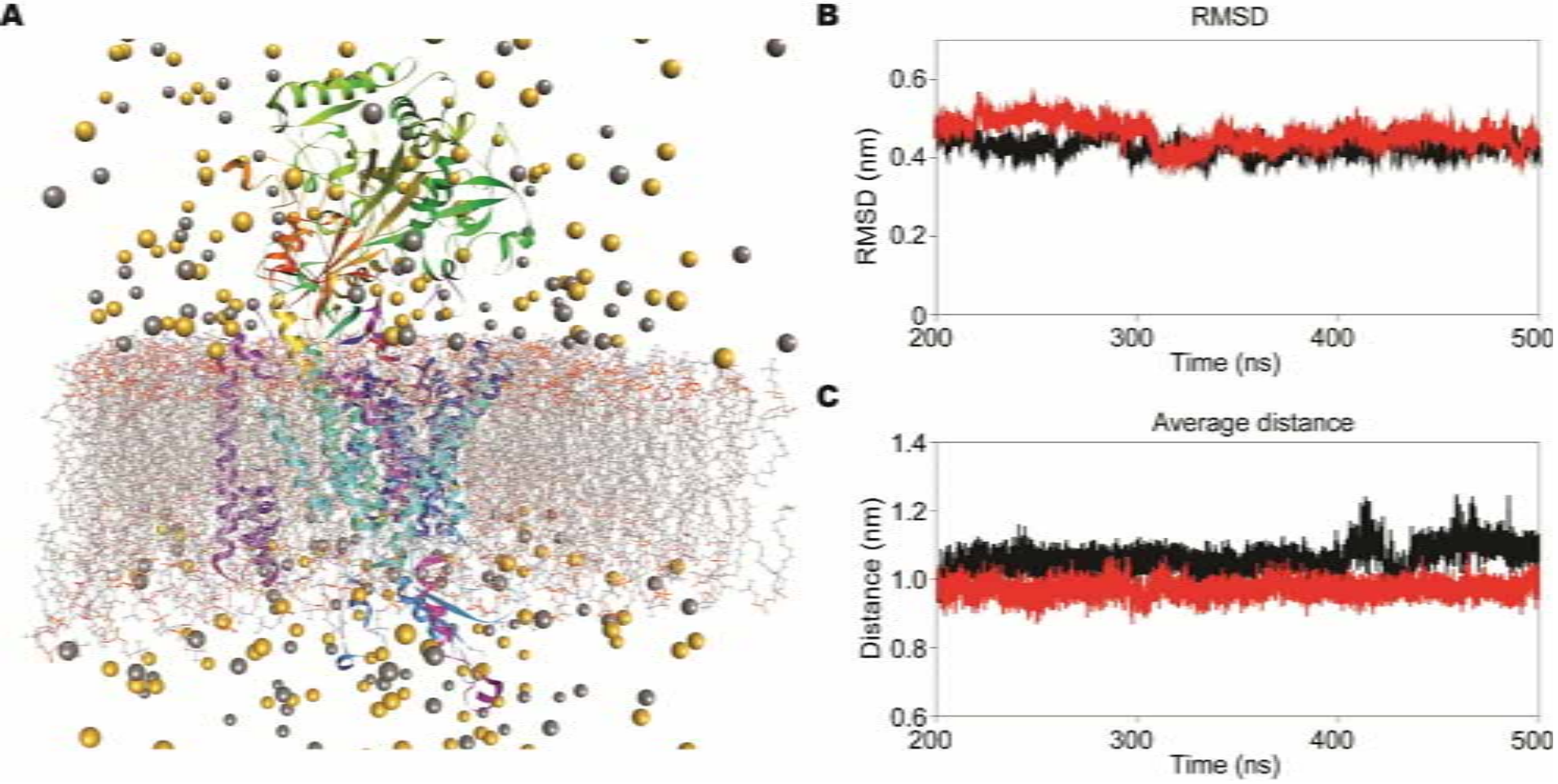
A
B
RMSD
RMSD (nm)
0.6
0.4
0.2
0
200
300
400
500
Time (ns)
C
Average distance
Distance (nm)
1.4
1.2
1.0
0.8
0.6
200
300
400
500
Time (ns)

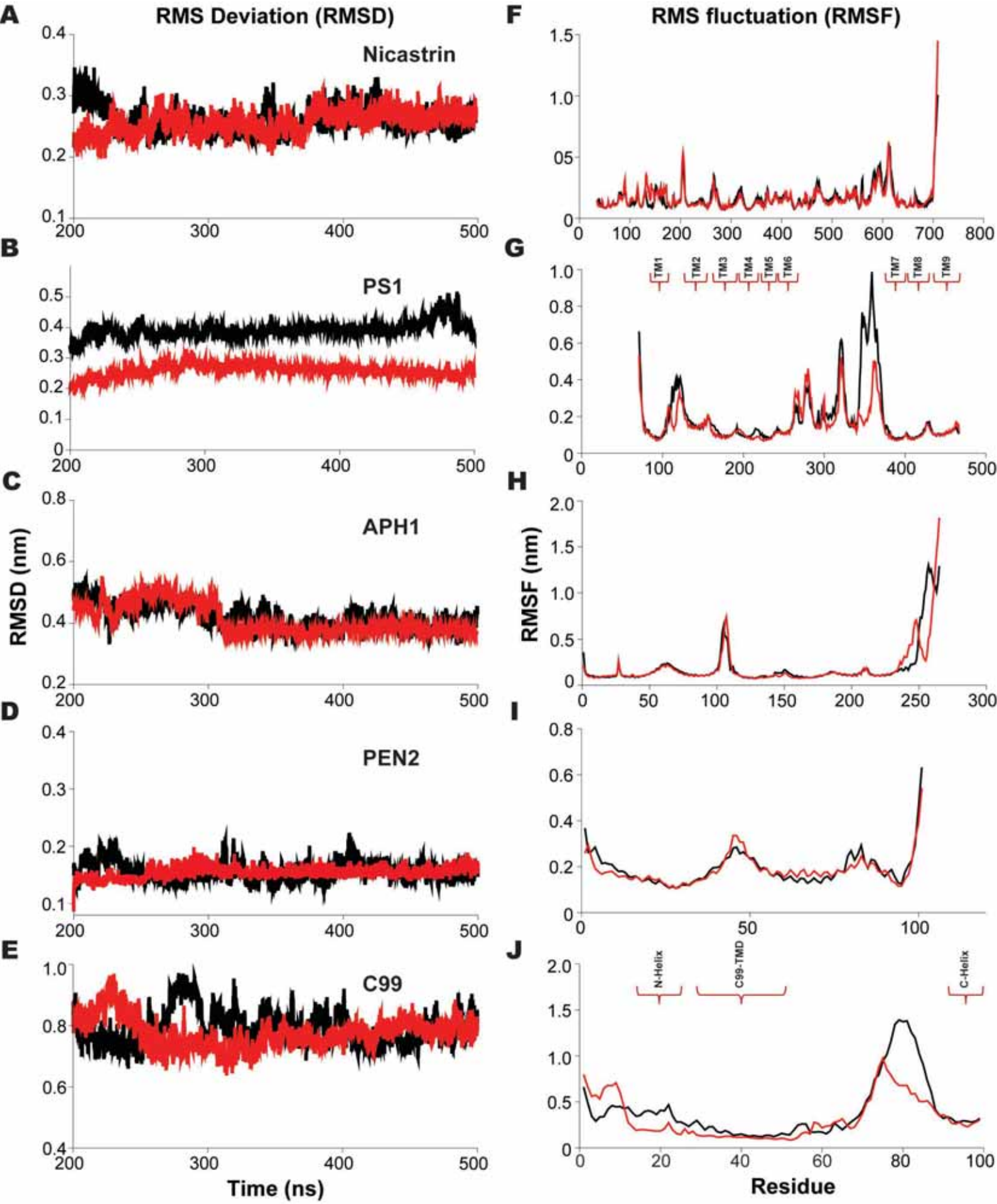
A
RMS Deviation (RMSD)
Nicastrin
B
PS1
C
APH1
D
PEN2
E
C99
RMSD (nm)
Time (ns)
F
RMS fluctuation (RMSF)
G
TM1
TM2
TM3
TM4
TM5
TM6
TM7
TM8
TM9
H
RMSF (nm)
I
J
N-Helix
C99-TMD
C-Helix
Residue

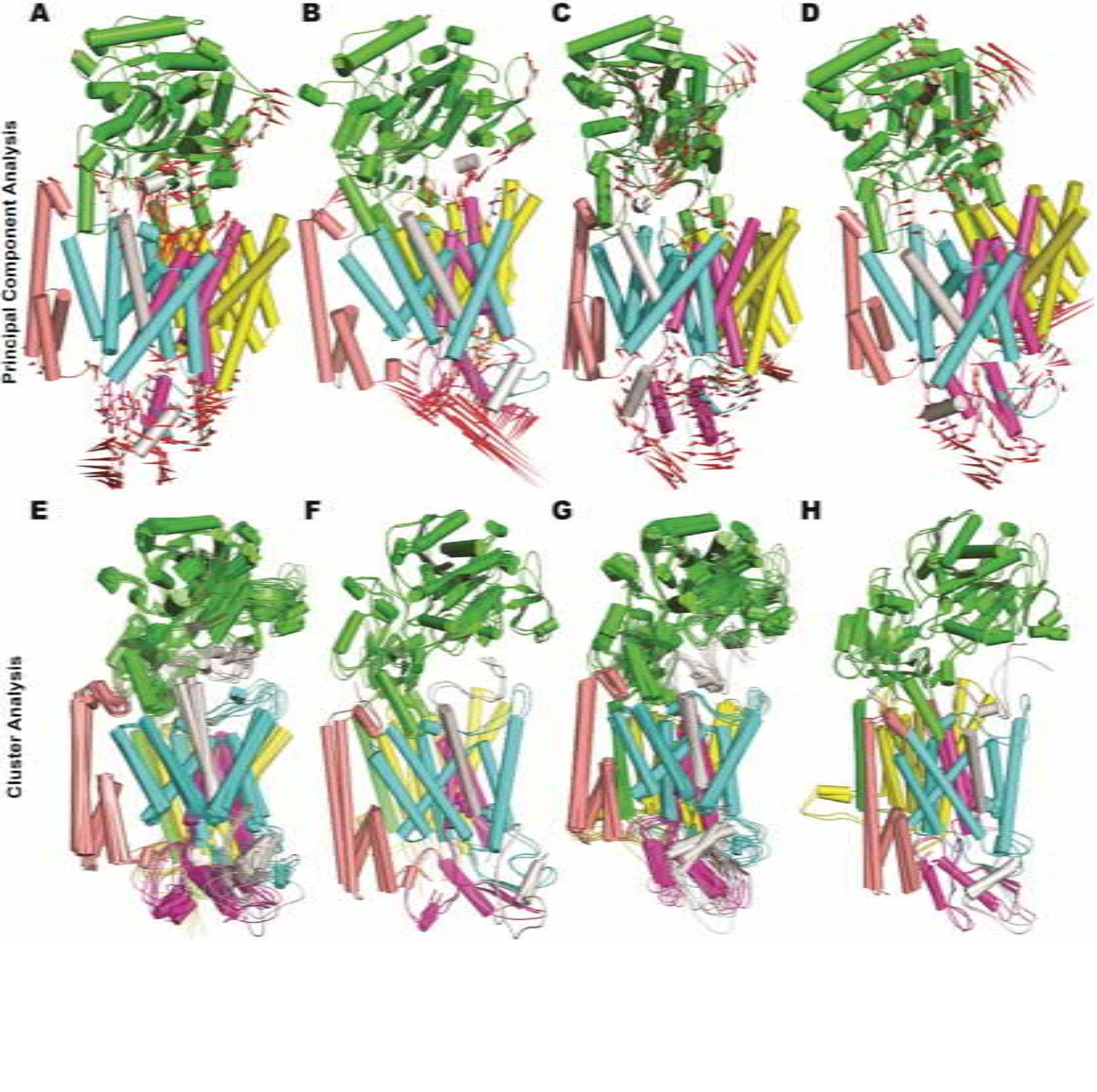
A
B
C
D
Principal Component Analysis
E
F
G
H
Cluster Analysis

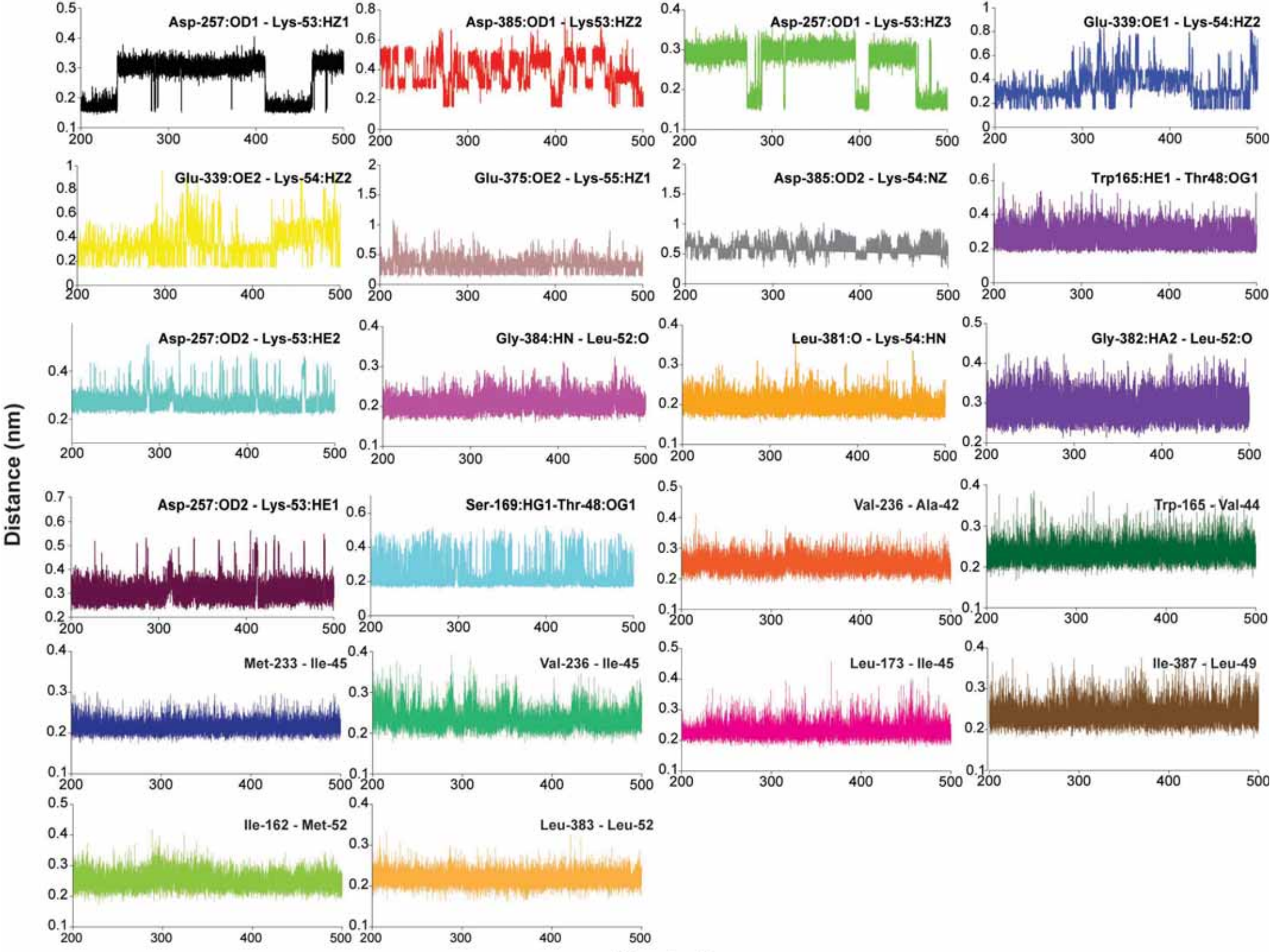
Asp-257:OD1 - Lys-53:HZ1
Asp-385:OD1 - Lys53:HZ2
Asp-257:OD1 - Lys-53:HZ3
Glu-339:OE1 - Lys-54:HZ2
Glu-339:OE2 - Lys-54:HZ2
Glu-375:OE2 - Lys-55:HZ1
Asp-385:OD2 - Lys-54:NZ
Trp165:HE1 - Thr48:OG1
Asp-257:OD2 - Lys-53:HE2
Gly-384:HN - Leu-52:O
Leu-381:O - Lys-54:HN
Gly-382:HA2 - Leu-52:O
Asp-257:OD2 - Lys-53:HE1
Ser-169:HG1-Thr-48:OG1
Val-236 - Ala-42
Trp-165 - Val-44
Met-233 - Ile-45
Val-236 - Ile-45
Leu-173 - Ile-45
Ile-387 - Leu-49
Ile-162 - Met-52
Leu-383 - Leu-52
Distance (nm)
Time (ns)

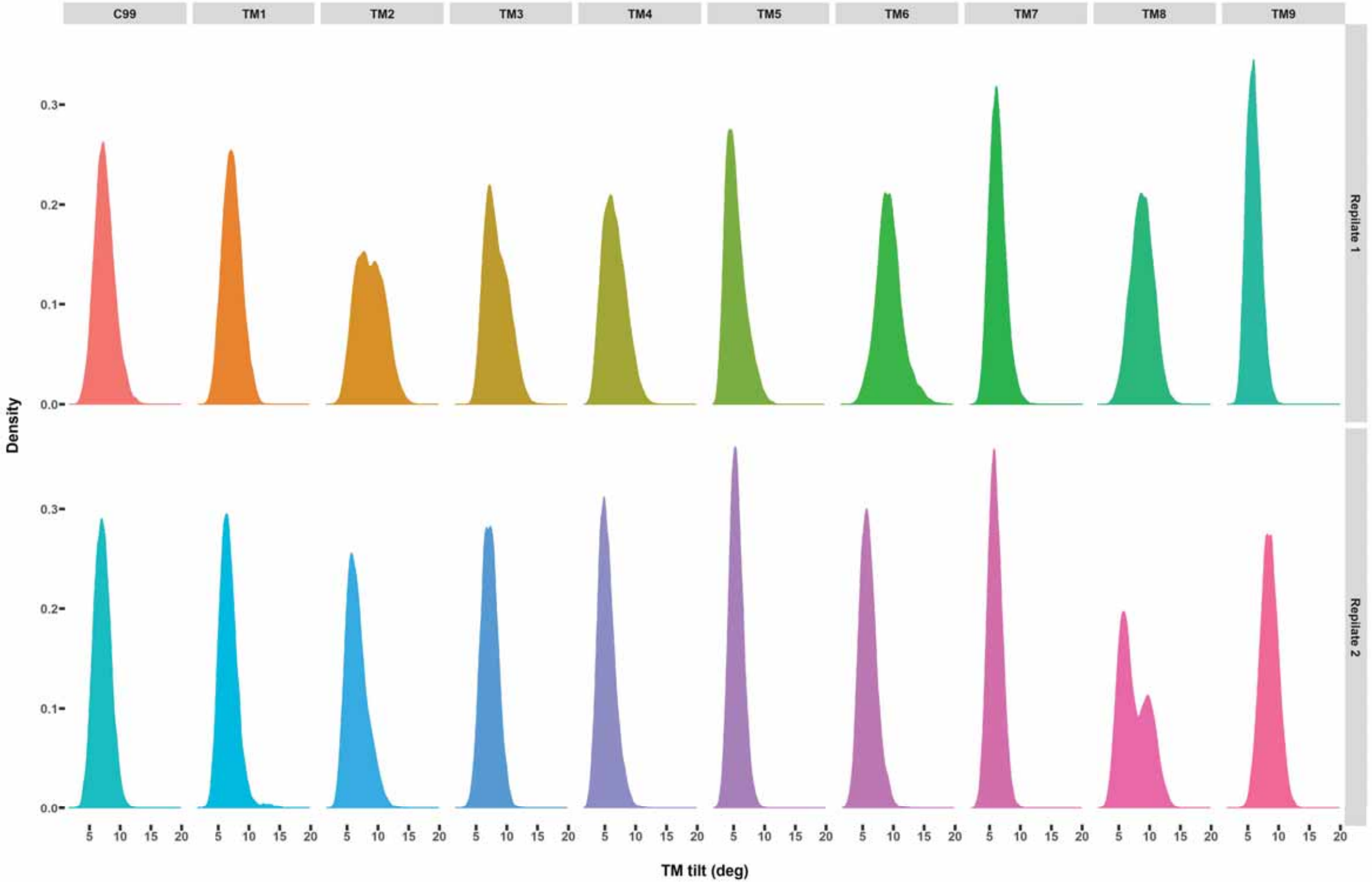
C99
TM1
TM2
TM3
TM4
TM5
TM6
TM7
TM8
TM9
Replate 1
Replate 2
Density
0.0
0.1
0.2
0.3
5
10
15
20
TM tilt (deg)

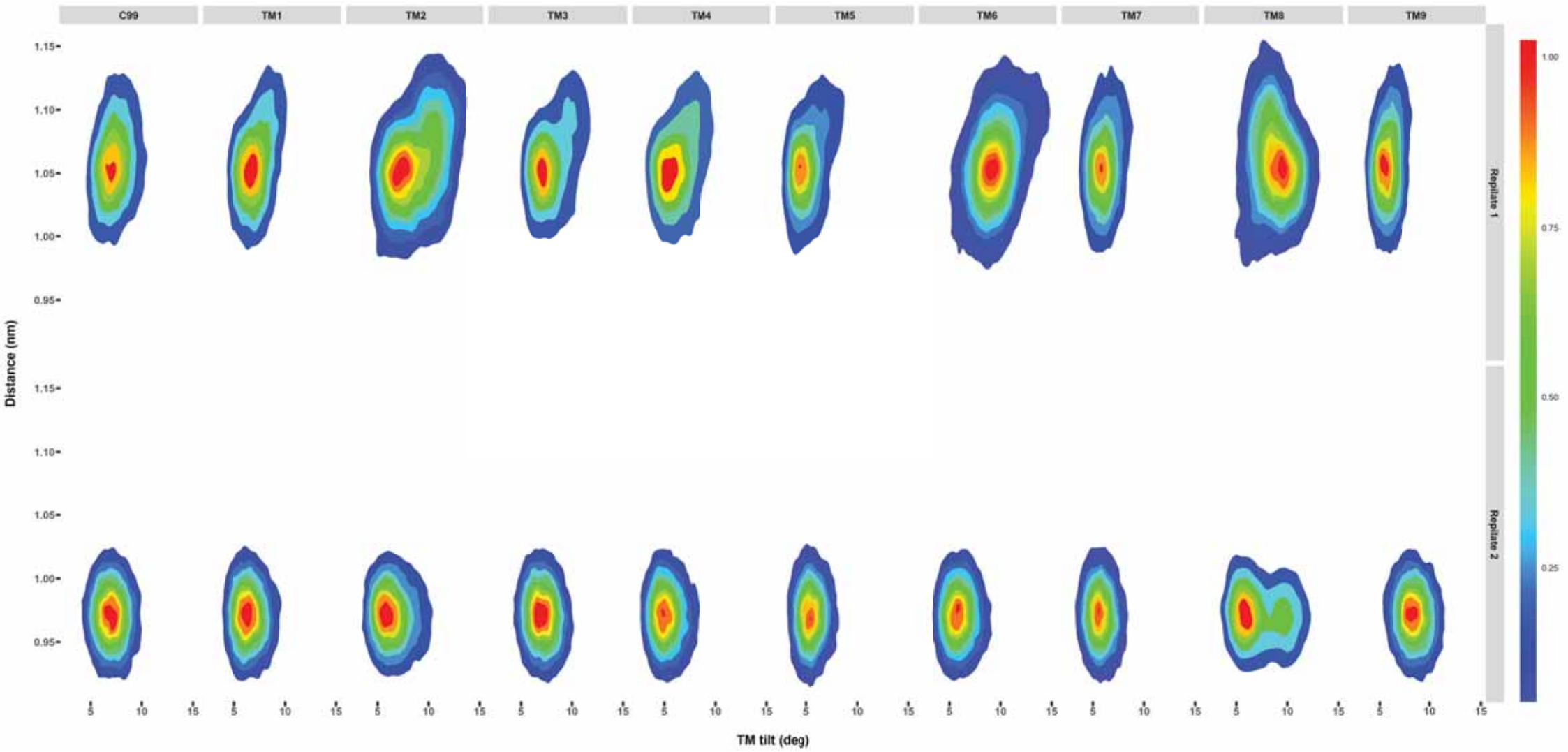
C99
TM1
TM2
TM3
TM4
TM5
TM6
TM7
TM8
TM9
Distance (nm)
1.15
1.10
1.05
1.00
0.95
Replicate 1
Replicate 2
1.00
0.75
0.50
0.25
5
10
15
TM tilt (deg)

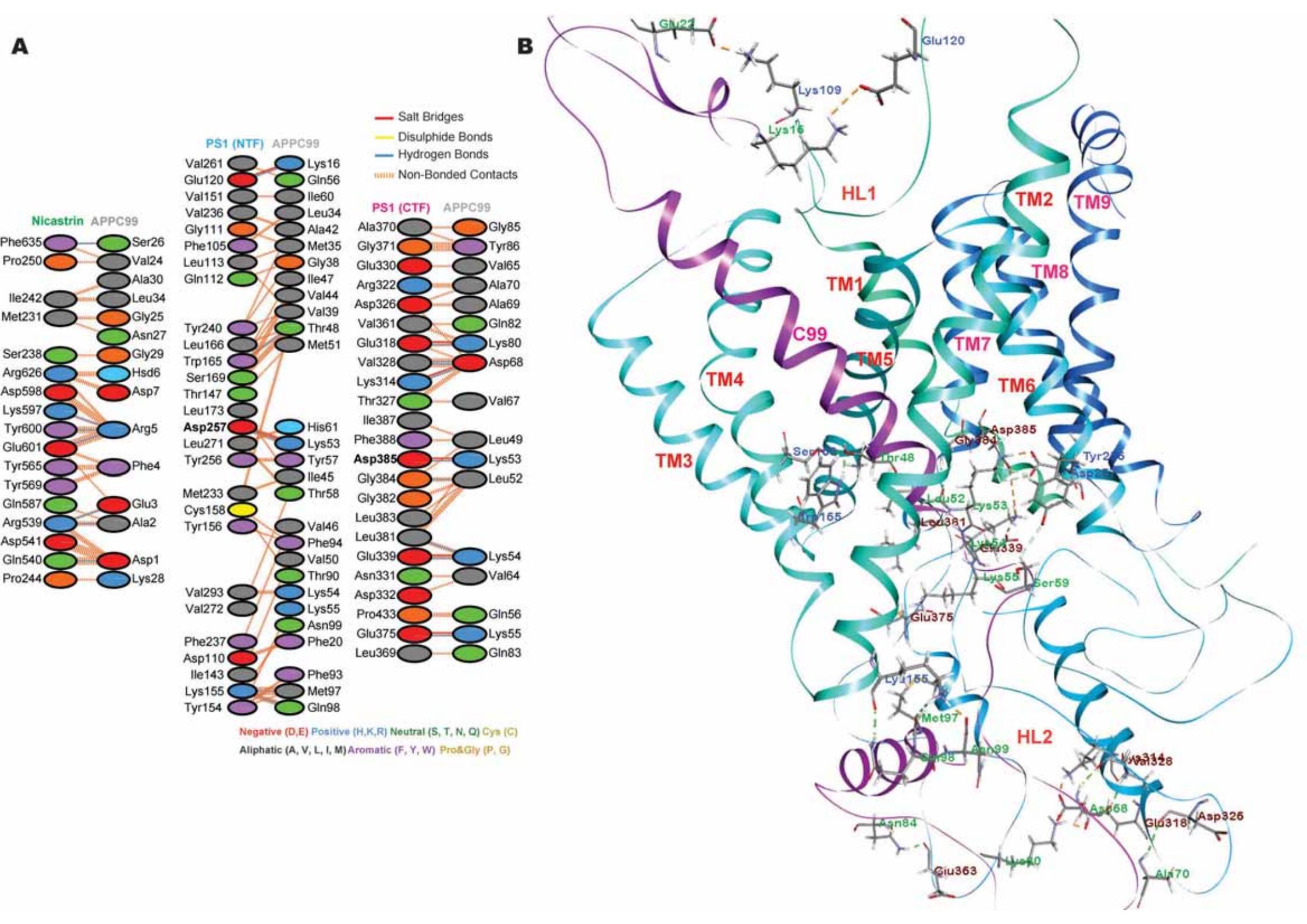
A
Nicastrin APPC99
Phe635 Ser26
Pro250 Val24
Ala30
Ile242 Leu34
Met231 Gly25
Asn27
Ser238 Gly29
Arg626 Hsd6
Asp598 Asp7
Lys597
Tyr600 Arg5
Glu601
Tyr565 Phe4
Tyr569
Gln587 Glu3
Arg539 Ala2
Asp541
Gln540 Asp1
Pro244 Lys28
PS1 (NTF) APPC99
Val261 Lys16
Glu120 Gln56
Val151 Ile60
Val236 Leu34
Gly111 Ala42
Phe105 Met35
Leu113 Gly38
Gln112 Ile47
Val44
Val39
Tyr240 Thr48
Leu166 Met51
Trp165
Ser169
Thr147
Leu173
Asp257 His61
Leu271 Lys53
Tyr256 Tyr57
Ile45
Met233 Thr58
Cys158
Tyr156 Val46
Phe94
Val50
Thr90
Val293 Lys54
Val272 Lys55
Asn99
Phe237 Phe20
Asp110
Ile143 Phe93
Lys155 Met97
Tyr154 Gln98
PS1 (CTF) APPC99
Ala370 Gly85
Gly371 Tyr86
Glu330 Val65
Arg322 Ala70
Asp326 Ala69
Val361 Gln82
Glu318 Lys80
Val328 Asp68
Lys314
Thr327 Val67
Ile387
Phe388 Leu49
Asp385 Lys53
Gly384 Leu52
Gly382
Leu383
Leu381
Glu339 Lys54
Asn331 Val64
Asp332
Pro433 Gln56
Glu375 Lys55
Leu369 Gln83
Salt Bridges
Disulphide Bonds
Hydrogen Bonds
Non-Bonded Contacts
Negative (D,E) Positive (H,K,R) Neutral (S, T, N, Q) Cys (C)
Aliphatic (A, V, L, I, M) Aromatic (F, Y, W) Pro&Gly (P, G)
B
Glu22
Glu120
Lys109
Lys16
HL1
TM2
TM9
TM1
TM8
C99
TM5
TM7
TM4
TM6
TM3
Asp385
Gly384
Thr48
Leu52
Lys53
Leu381
Glu339
Lys55
Ser59
Glu375
Lys155
Met97
HL2
Ser98
Asn99
Asn84
Glu363
Asp68
Glu318
Asp326
Ala70